INSTITUTO SUPERIOR DE ENGENHARIA DO PORTO
MESTRADO EM ENGENHARIA BIOMÉDICA



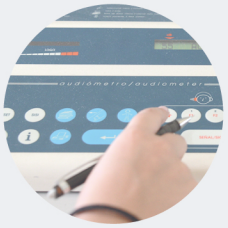


Preparation and characterisation of kefiran, a promising natural polymer for biomedical applications

MARIA DANIELA ALVES MENEZES
novembro de 2022

Preparation and characterisation of kefiran, a promising natural polymer for biomedical applications

Maria Daniela Alves Menezes

Biomedical Engineer from Instituto Superior de Engenharia do Porto

"Dissertation presented at the Instituto Superior de Engenharia do Porto to obtain a Master's degree in Biomedical Engineering"

Supervisor: Cristina Ribeiro, PhD

Co-Supervisor: Paula Parreira, PhD

November 2022

“You never know how strong you are until being strong is the only choice you have.”

Bob Marley

Acknowledgements

The development of this project would not be possible without the collaboration, encouragement and effort of different parties. In this regard, I would like to express all my gratitude and appreciation to all those who, directly or indirectly, contributed to making this task a reality. I would like to express my sincere thanks to everyone.

First of all, I want to thank my advisors, Professor Cristina Ribeiro and Doctor Paula Parreira, for the motivation, support and permanent availability throughout this process. Moreover, thanks to i3S for allowing me to do my thesis in their facilities.

To my family, especially to my Parents, Sister and Brother, thanks for this opportunity, for encouraging me to fight for my goals and for always believing in me, even when it is difficult for me to do so.

I would like to give a word of appreciation to Marta, Catarina and my other friends for being my support and company, for motivating me and helping me at all times.

A special thanks to Diana and Mariana for always being available to help me when I needed it. Furthermore, I would like to acknowledge the support of Dr. Ricardo Vidal, Dr. Claúdia Machado, Eng. Paula Venda and Dr. Sofia Quintas in the characterisation techniques.

Finally, I would like to leave my thanks to ISEP and all the Professors who accompanied me throughout my academic career, for the help, patience and teachings passed along these five years.

Resumo

O kefiran é um exopolissacarídeo presente nos grãos de kefir, sintetizado por várias espécies de *Lactobacillus*. Este polímero natural tem várias propriedades biológicas interessantes, de entre as quais se destacam as propriedades antibacterianas.

A *Helicobacter pylori* é uma bactéria Gram negativa que infecta o estômago de cerca de 50% da população mundial. É o agente etiológico de várias patologias, como gastrite crónica e é responsável por 90% dos casos de cancro gástrico. A terapia disponível, baseada em antibióticos, é ineficaz em cerca de 20 a 40% dos casos, sobretudo pela elevada taxa de resistência.

Este trabalho focou-se na otimização de um método de extração do kefiran, sua caracterização e desenvolvimento de micro/nanopartículas para avaliação do seu efeito contra a *H. pylori* J99 e 26695. Para tal, alginato ultrapuro foi usado na preparação das nanopartículas devido à sua capacidade de reticular na presença de iões divalentes, permitindo, quando misturado com kefiran, a obtenção de nanopartículas (~100 nm) usando técnicas de microfluídica. Foram também desenvolvidas nanopartículas com um péptido antimicrobiano (MSI-78) com efeito contra a *H. pylori*. A segurança desta estratégia de bioengenharia foi ainda avaliada em bactérias representativas do microbioma gastro-intestinal, *Escherichia coli* e a *Lactobacillus acidophilus*.

As nanopartículas de kefiran e alginato sem péptido não tiveram atividade antimicrobiana. Além disso, as nanopartículas com péptido também não demonstraram efeito, sugerindo assim que a libertação do péptido não ocorreu.

A citotoxicidade do kefiran contra células do adenocarcinoma gástrico humano foi avaliada (ISO 10993-5;12) e não foi reportada citotoxicidade.

Visando o uso de kefiran em aplicações de engenharia de tecidos, foram preparados scaffolds porosos através da técnica de liofilização, tendo sido obtidos scaffolds com estrutura porosa interligada.

Os resultados obtidos fornecem novos conhecimentos sobre um polímero natural ainda pouco explorado e potencialmente muito interessante para aplicações biomédicas.

Palavras-chave: Kefiran; Alginato; Nanopartículas; *Helicobacter pylori*; Péptido; Discos; Scaffold.

Abstract

Kefiran is an exopolysaccharide present in kefir grains, which is synthetised by various *Lactobacillus* species. This natural polymer has several interesting biological properties, among which the antimicrobial properties stand out.

Helicobacter pylori is a Gram-negative bacterium that infects the stomach of about 50% of the world's population. It is the etiologic agent of several pathologies, such as chronic gastritis and is responsible for 90% of gastric cancer cases. The available therapy, based on antibiotics, is ineffective in about 20-40% of cases, mainly due to high rate of resistance.

This work focused on the optimization of a kefiran extraction method, its characterisation and development of micro/nanoparticles to evaluate its effect against *H. pylori* strains J99 and 26695. For this, ultrapure alginate was used in the preparation of nanoparticles due to its ability to crosslink in the presence of divalent ions, allowing, when mixed with kefiran, to obtain nanoparticles (~100 nm) using microfluidics techniques. Nanoparticles loaded with an antimicrobial peptide (MSI-78) with effect against *H. pylori* were also developed. The safety of this bioengineering strategy was further evaluated in bacteria representative of the gastrointestinal microbiome, *Escherichia coli* and *Lactobacillus acidophilus*.

Kefiran and alginate nanoparticles non-loaded with MSI-78 peptide had no antimicrobial activity. Moreover, the nanoparticles loaded with MSI-78 also showed no effect, thus suggesting that peptide release did not occur.

The cytotoxicity of kefiran against human gastric adenocarcinoma cells was evaluated (ISO 10993-5;12) and no cytotoxicity was reported.

Envisaging the possibility of using kefiran in tissue engineering applications, porous scaffolds were prepared using the freeze-drying technique and scaffolds with interconnected porous structure were obtained.

The results achieved provide new insights into a natural polymer still little explored that is potentially very interesting for biomedical applications.

Key words: Kefiran; Alginate; Nanoparticles; *Helicobacter pylori*; Peptide; Discs; Scaffold.

List of Contents

List of Figures

List of Tables

List of Symbols and Abbreviations

A	Absorbance
AGS	Human Gastric Adenocarcinoma
AMP	Antimicrobial peptide
AST	Antibiotic Susceptibility Testing
BA	Blood Agar
CagA	Cytotoxin-associated gene A
CFUs/mL	Colony-Forming Units per millilitre
CRM	Confocal Raman Microscopy
DTH	Delayed-type hypersensitivity
DSC	Differential Scanning Calorimetry
EDTA	Ethylenediaminetetraacetic acid
EKA	Electrokinetic analyser
FBS	Fetal Bovine Serum
FTIR	Fourier-Transform Infrared Spectroscopy
Gal	Galactose
Glu	Glucose
IR	Infrared Radiation
ISEP	Instituto Superior de Engenharia do Porto
ISO	International Organization for Standardization
LSPR	Localized Surface Plasmon Resonance
MRS	De Man, Rogosa and Shape
NP	Nanoparticles
NTA	Nanoparticle Tracking Analysis

OD	Optical density
PBS	Phosphate-Buffered Saline
PPI	Proton Pump Inhibitor
RPM	Revolutions Per Minute
RPMI	Roswell Park Memorial Institute
RT	Room Temperature
RT-PCR	Real-time polymerase chain reaction
RUT	Rapid Urease Test
SEM	Scanning Electron Microscopy
T	Transmittance
TEM	Transmission Electron Microscopy
TGA	Thermogravimetric Analysis
TSA	Trypticase Soy Agar
UV	Ultraviolet
VacA	Vacuolating cytotoxin A
ZP	Zeta Potential

CHAPTER 1 – INTRODUCTION

1. Introduction

The present report describes the work developed during the thesis and was carried out within the scope of the MSc in Biomedical Engineering fostered by ISEP, in the academic year of 2021/2022.

This project was developed at INEB/i3S with the collaboration of the Microenvironments for New Therapies and Bioengineered Surfaces groups.

1.1. Objective of the work

The main objective of this work was to optimize the kefiran extraction process, develop kefiran nanoparticles and address its use within *Helicobacter pylori* infection management. To this end, polymeric nanoparticles of kefiran/alginate were developed and their effect against this gastric bacterium was studied. In addition, the impact of these particles on bacteria representative from the gut microbiome was also evaluated.

1.2. Report organization

Initially, an overview on kefir and kefiran is given, with the latter being divided into several topics for a deeper overview of this exopolysaccharide and its use in biomedical applications. Then, the materials and methods developed and applied in this work are presented. The following chapter concerns the obtained results and discussion. The last chapter is the overall conclusion, also alluding to work limitations and possible improvements in future projects.

CHAPTER 2 – BACKGROUND

2. Background

In this section, an overview on kefir, kefiran and *Helicobacter pylori* is given. In addition, material characterization techniques as well as particle production techniques are addressed.

2.1. Kefir

Kefir, a sour, refreshing, probiotic, mildly alcoholic, acidic fermented milk drink, consists of a stimulating and self-carbonated drink obtained through the mixed alcoholic and lactic fermentation of kefir grains [1-3]. Typically, kefir is made from cow's milk but different milk types have been tested in the manufacture of kefir, namely plant-based (peanut milk and soy milk) and other animal-based (ewe milk and buffalo milk). As such, kefir can be distinguished as dairy and non-dairy, depending on the type of substrate used for fermentation. Dairy kefir is obtained by the fermentation of lactose in milk, carried out by bacteria and yeasts that are naturally present in kefir grains, while non-dairy kefir is prepared by fermenting kefir grains with a sugar solution, usually brown sugar [3]. Still, these two types of kefir are similar in terms of structure, related microorganisms and the metabolic products obtained during the fermentation process. Kefir grains are added to milk and left to ferment at 20-25 ºC for 18-24 hours. During the fermentation, the grains biomass increases and these can split into new, smaller grains and release viable cells into the substrate [1]. Finally, these grains are removed from the kefir produced through sieving and the grains are re-used for the next inoculation [3].

Kefir grains are composed by water, lipids, proteins, sugar and ash [2].These consist of a bond of many exopolysaccharides, namely kefiran with bacteria, such as lactic acid bacteria and numerous yeasts, combined with casein within a polysaccharide matrix [2, 4]. An exopolysaccharide is a structurally and functionally important biopolymer that is secreted by various prokaryotic and eukaryotic microorganisms, in response to biotic or abiotic stresses and to survive in extreme environments [5].

2.2. Kefiran

Kefiran is a clear or pale-yellow slimy exopolysaccharide produced by the microflora of kefir grains [Figure 1a and 1b], representing more than half of dry weight [6, 7].

It has 127 hexose units, with approximately the same amount of galactose (Gal) and glucose (Glu) residues in the chain sequence [Figure 1c] [8, 9]. Furthermore, kefiran molecular weight is in the 50 to 15,000 kilodalton (kDa) range, depending on the carbon source, purification and conditions of isolation [10].

Kefiran can degrade to various non-hazardous polysaccharide intermediates and, eventually, to D-glucose and D-galactose (marked in red and blue, respectively, between the configuration of these two molecules in [Figure 1c]). This occurs through a series of slow enzymatic degradation processes, in which variable glycosidic linkages are broken between the glucose and galactose units present in kefiran [11].

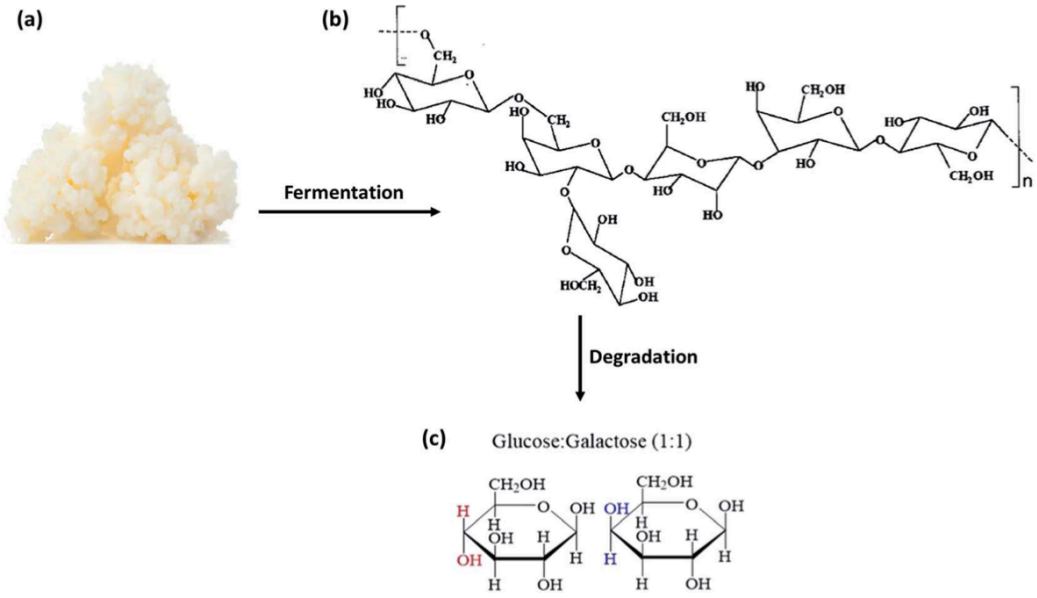

Figure 1. (a) Kefir grains; (b) Chair configuration of the proposed molecular structure of kefiran after kefir fermentation; (c) Chemical structures of its constituent monomers (glucose and galactose) upon enzymatic degradation of kefiran. D-glucose and D-galactose marked in red and blue, respectively. Adapted from [11].

Through the analysis of the kefiran chemical structure, it is possible to observe that it consists of a branched hexa- or hepta-saccharide repeating units, composed of a regular pentasaccharide unit, to which one or two sugar residues are randomly attached [Figure 3] [7].

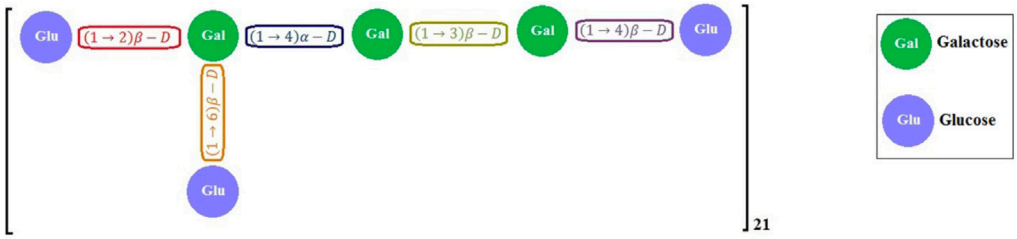

Figure 2. Chemical structure of kefiran. Adapted from [9].

Kefiran backbone is composed by (1→6)-linked Glu, (1→3)-linked Gal, (1→4)-linked Gal, (1→4)-linked Glu and (1→2,6)-linked Gal, where the Glu branches are linked to the O-2 of the Gal residues. The backbone ends with a residue of Glu [Figure 2] [12].

2.2.1. Kefiran extraction

Kefiran present in kefir grains is synthetised by various *Lactobacillus* species, namely *L. kefiranofaciens*, *L. kefirgranum*, *L. parakefir*, *L. kefir* and *L. delbrueckii* sp *bulgaricus* [7]. *L. kefiranofaciens*, a milk bacterium, is considered to be the largest producer of kefiran [12].

In the literature, the production of kefir and kefiran through fermentation is reported to have higher yield when the temperature is between 20 and 30 ºC and the pH is between 5 and 6. Moreover, after the culture of microorganisms has been chosen, it is necessary to create the most appropriate medium and for that, nitrogen sources (yeast extract, peptone, meat extract and casein hydrolysate) and carbon sources (mannitol, sucrose, lactose and glucose) have also been subject of optimization and research [13]. Among the various carbon sources, lactose is considered the best for kefiran production [10].

After selecting the proper fermentation conditions, the next two steps are the kefiran isolation and purification. A possible methodology is the one described as follows: kefir grains are added to hot water (60-90 ºC), under controlled agitation, temperature and time. After this, the mixture must be cooled and centrifuged to remove microbial cells and proteins. The polysaccharide dissolved in the supernatant is then added to cold ethanol at -20 ºC. Then, this mixture undergoes centrifugation and the kefiran-rich pellets are dissolved in hot (60 ºC) distilled water. This purification process is repeated twice to obtain a purified kefiran solution. Finally, the resulting precipitate is dried in an oven [Figure 3] [13].

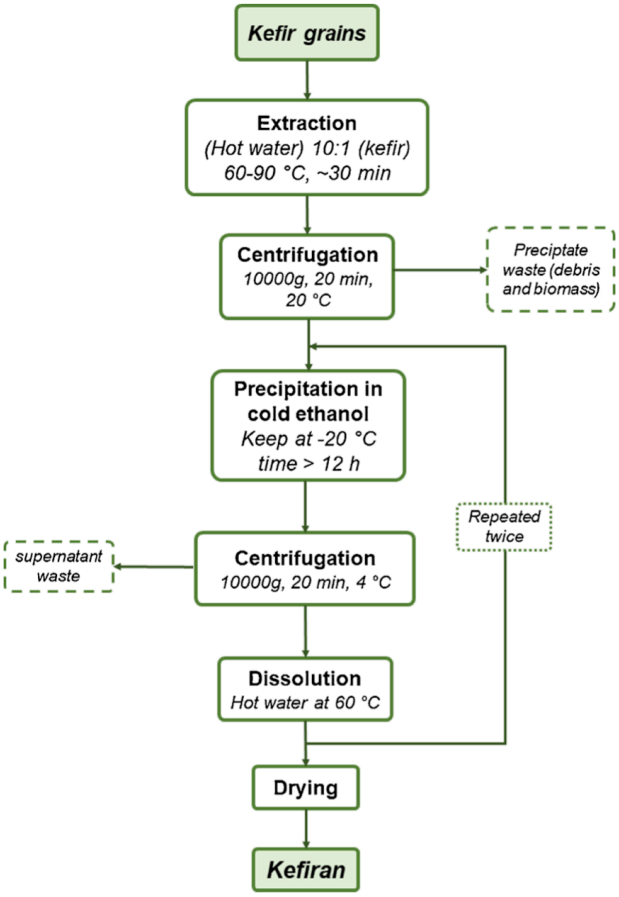

Figure 3. Simplified flowchart with the main steps of the Kefiran extraction and purification procedures described in the literature. Adapted from [13].

Currently, kefiran production is inefficient and only allows a small-scale production. The extraction of kefiran from kefir has some disadvantages, such as low yield and variations between kefir batches. Large-scale kefiran applications demand a more economical and efficient manufacturing process. As such, bioreactors have been evaluated to increase kefiran production on a semi-industrial scale [11].

2.2.2. Kefiran's properties

Kefiran has several benefits for human health, which has contributed significantly to the global growing interest on this biopolymer [14]. Table 1 presents an overview of general relevant properties of kefiran and its applications, highlighting its versatile nature.

Table 1. Kefiran properties and application.

Property	Description	Reference
Hydrophilic nature	• High tendency to adsorb moisture	[7]
Gelling agent	• As a result of a cryogenic treatment	[15]
Modulator of the gut immune system	• Protects the epithelial cells against *Bacillus cereus* toxin • Promote *in vitro* growth of a *Bifidobacterium bifidum* strain	[15] [16]
Antitumor	• Correlation between the delayed-type hypersensitivity (DTH) response and antitumor activity	[17]
Anti-inflammatory	• Significantly inhibits the formation of granuloma tissue • Nitric oxide scavenging in a cell-free system	[18] [14]
Antioxidant	• Reducing power • Metal chelating • Hydroxyl and superoxide radical scavenging	[14]
Antimicrobial	• Inhibits the growth of Gram-positive, Gram-negative bacteria and the yeast • Has nisin as the antibacterial lantibiotic	[15] [11]
Wound healing	• Encapsulation and delivery of platelets in kefiran can be applied in surface bleeding treatment	[7]
Able to decrease the serum cholesterol level	• Traps enterohepatics-circulating cholesterol in the intestine	[19]

2.2.3. Kefiran's applications

Due to the relevant properties of kefiran, it can be used in different fields, ranging from food to tissue-engineering and health-related applications. Regarding food applications, as kefiran has texture and gelling properties, it is used in the preparation of biofilms for food packaging, to provide the desired rheological properties for dairy products, or use as a thickener [1]. Over the next sections, more details are given on the biomedical engineering area, namely on biomedical applications and tissue engineering [7].

2.2.3.1. Tissue engineering

Regenerative engineering is the artificial production of cellular tissue. For this, it is essential that there are synergistic effects between cells, growth factors and scaffolds. Scaffolds containing kefiran are biodegradable and their degradation produces products recognized as safe, thus exhibiting safety and quality features. Also, due to the possibility of controllable 3D morphology and remarkable mechanical properties, kefiran scaffolds are promising materials in the field of tissue engineering [Figure 4] [11].

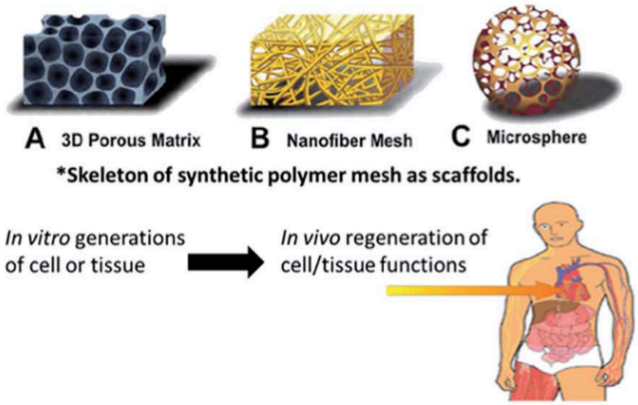

Figure 4. Kefiran scaffolds can take form of (a) three-dimensional porous matrix; (b) nanofibrous mesh and; (c) hollow microsphere for cell growth and proliferation. Adapted from [11].

Radhouani *et al.* developed a kefiran-based 3D scaffold using the free gelling technique for tissue engineering. Stem cells derived from human adipose tissue were grown on this scaffold and, after 72 hours, they were still metabolically active. The scaffold had a porous 3D matrix, high stability and flexible behaviour, which are fundamental aspects for any scaffold [20].

Ghasemlou *et al.* produced kefiran films with good strength and elongation, which suggests that kefiran polymeric matrices can be prepared with desirable characteristics. The films were fabricated from pure kefiran with the use of plasticizers such as sorbitol and glycerol [21].

In addition, kefiran also demonstrates wound healing properties and can be a suitable scaffold material due to its biocompatible and biodegradable properties, as well as its ideal surface characteristics, porosity, mechanical strength and geometry. Thus, natural polymers like kefiran are among the top choice of biodegradable support materials due to their polymer-cell interactions and lack of immune responses and toxicity [11].

2.2.3.2. Drug/probiotic delivery systems

Oral intake of drugs continues to be the most used route of administration due to its non-invasive character and convenience for the patient [22]. Also, it allows for the local and systematic delivery of a wide range of molecules, from small to biomacromolecules. However, oral administration has some limitations, such as low solubility, low permeability, rapid degradation in the gastrointestinal tract and inability to penetrate the protective mucosal barrier [23]. Several attempts to overcome these issues have focused on understanding the physiology of the gastrointestinal tract, in both healthy and diseased stages. Innovative pharmaceutical approaches have also been explored to improve regional drug targeting in the gastrointestinal tract, including nanoparticle formulations with encapsulated drugs [24].

The use of kefiran as a basis to produce thin films or biopharmaceutical drug delivery vehicles allows to improve the pharmacodynamics and pharmacokinetics of encapsulated drugs. This makes possible to speed up recovery or even improve the individual general well-being. Besides that, kefiran is non-digestible and non-absorbable in the stomach because it is resistant to its acidic conditions and digestive enzymes [11].

A study by Piermaria *et al.* showed the effectiveness of edible kefiran films as carriers of live probiotic microorganisms such as *Lactobacillus plantarum* CIDCA 8327 and *Kluyveromyces marxianus* CIDCA 8154 to the small intestine. The experimental results revealed that the film was able to preserve the viability of the probiotics, only showing residual loss after 35 days of storage at 20 ºC [16].

Also, the encapsulation of the microorganisms within the kefiran film did not alter their physicochemical and biological properties, conferring protection against the acidic environment of the stomach. Thus, kefiran films have excellent potential as vehicles to deliver probiotics in situations of gastrointestinal disorders [Figure 5] [11].

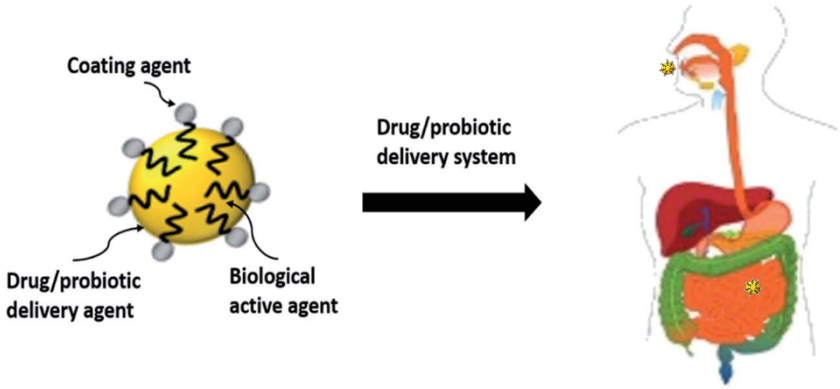

Figure 5. Use of kefiran for encapsulation of probiotics and drugs for gastro-intestinal delivery. Adapted from [11].

Serafini *et al.* indicated the efficiency of kefiran in increasing the growth of the *Bifidobacterium bifidum* PRL2010 strain by modulating its gene expression. Bifidobacteria are one of the main microorganisms that colonize the gastrointestinal tract of human infants. The experimental results showed that kefiran can influence the transcriptome of *Bifidobacterium bifidum* PRL2010, resulting in an increased transcription of genes involved in the metabolism of dietary glycans, as well as genes that act as host-microbe effector molecules. Therefore, kefiran can contribute considerably to probiotic therapy [25].

Recently, kefiran and alginate gel microspheres have been developed to carry the antibiotic ciprofloxacin. Blandón *et al*. encapsulated ciprofloxacin in kefiran and alginate microspheres with an encapsulation efficiency of 80 % [15]. This system allowed for the controlled release of the drugs and enhanced its bactericidal effect against common pathogens, such as *Escherichia coli*, *Klebsiella pneumoniae*, *Pseudomonas aeruginosa*, *Staphylococcus aureus* and *Salmonella typhymurium* [15].

2.3.Characterisation techniques

To analyse the properties of the kefiran produced and respective nanoparticles and porous scaffolds, several characterisation techniques namely, Fourier-Transform Infrared Spectroscopy, Differential Scanning Calorimetry, Thermogravimetric Analysis, Zeta Potential and Nanoparticle Tracking Analysis were used. In the following subsections a brief explanation of the techniques used is presented.

2.3.1. Fourier-Transform Infrared Spectroscopy (FTIR)

Fourier-Transform Infrared Spectroscopy (FTIR) is a vibrational technique used to identify the functional groups and chemical bonds present in the material, using a beam of infrared radiations. It measures the absorption of infrared radiation (IR) made by infrared active bonds in the molecule at varying wavelengths of light. As a result, it provides a spectrum which represents the percentage of transmittance (%T) or absorbance (A) versus wavenumber (cm^{-1}) that is the inverse of the wavelength [26].

2.3.2. Confocal Raman Microscopy (CRM)

Confocal Raman Microscopy (CRM) is a label-free, contact-free, non-invasive and non-destructive imaging technique, which can be applicable in aqueous environments. Confocal microscope provides excellent depth resolution and enables 3D Raman images and depth profiles to be acquired.

Raman effect is based on light interaction with the chemical bonds of a sample. The Raman spectrum comes from the vibrations of the chemical bonds, causing an energy shift in the backscattered light.

This technique is complementary to FTIR spectroscopy and allows the identification of the chemical and molecular compounds of the sample as well as the relative quantity of a specific component, stress and strain states. Crystallinity or types of polymorphic structures can also be determined. High-resolution confocal microscopes provide the information of a complete Raman spectrum at each image pixel and reach lateral resolution at the diffraction limit (1/2 of the excitation wavelength) [27].

The intensity of each peak in the Raman spectrum is directly related to the amount of each material that composes the sample and the position that each peak occupies in the spectrum is related to a specific type of component [28].

2.3.3. Differential Scanning Calorimetry (DSC)

Differential Scanning Calorimetry is a technique that allows the study of the thermal behaviour of substances to establish a relation between temperature and some of its specific physical properties. This technique measures the variation of the physical properties with time and temperature. DSC provides a measurement of the amount of energy absorbed or released by the sample as it heats up or cools down. Throughout a change in temperature, this technique measures the heat radiated or absorbed by the

sample, which is based on the temperature difference between the sample and the reference material [29], allowing to identify exo and endothermic transformations that may occur during heating.

2.3.4. Thermogravimetric Analysis (TGA)

Thermogravimetric Analysis is a technique that allows the measurement of the amount and rate of modification in the weight of a material as a function of temperature or time in an atmosphere of air, helium, nitrogen, other gas or in a vacuum. Firstly, the measurements are used to define the composition of the materials and to determine their thermal stability at temperatures up to 1200º C. Besides that, this technique allows the characterization of materials that present weight loss or gain because of decomposition, dehydration or oxidation. Materials such as polymers, metals, inorganic materials, plastics, ceramics, composite materials and glasses can be analysed through this technique [29].

2.3.5. Zeta Potential (ZP)

Zeta Potential (ZP) is a physical property which is exhibited by any material in suspension. ZP consists of an electric potential that materials develop in a solution through the creation of a double electrical layer. This technique is normally used to measure the surface charge and stability of the material [30].

ZP shows the degree of repulsion between the charged material in dispersion. Electrophoretic light scattering and electroacoustic determination are the techniques applied for the ZP analysis. Among these two, electrophoretic light analysis provides better resolution as well as more reliable results.

High ZP means highly charged particles, which prevents material aggregation due to electrical repulsion. On the other hand, when ZP is low, attraction overcomes repulsion, which can lead to aggregation [31].

2.3.6. Rheology

Rheology is the study of deformation and flow of matter, especially liquids and soft matter, when subjected to a force field. Rheological characterization of materials provides a general idea of the viscoelastic flow behaviour of the system. Moreover, this

analysis is very relevant to every material due to the fact that the rheological responses are closely related to final structures of the system [32].

Regarding polymers, its rheological behaviour is specially studied to investigate the structure and spatial arrangement of the material, providing information about the different intra- and inter-molecular interactions. Furthermore, it is the science of their flow in the melting state for thermoplastics and prior to cross-linking for the thermosets and elastomers [33].

2.3.7. Nanoparticle Tracking Analysis (NTA)

To characterize the size and concentration of the particles, the Nanoparticle Tracking Analysis (NTA) technique can be used. NTA is a multiparametric analytical technique with real-time visualization, scaling and counting. This technique is suitable for particles suspended in liquids with a size between 10 nm and 1 μm [34].

In short, particle size is determined by focusing a laser beam through a suspension of particles. The scattered light allows the visualization of the particles as well as the recording of their individual displacement over disjointed time intervals. The mean square displacement of each particle, the temperature and the viscosity of the liquid are necessary data to calculate individual particle sizes through the Stokes-Einstein equation. Concerning the concentration of particles, this is determined through the total count of particles and, later, it is represented as a binned histogram [35].

2.3.8. Scanning Electron Microscopy (SEM)

Scanning Electron Microscopy (SEM) is a technique used to characterise the morphology, topology and detailed surface structure of solid materials. SEM uses beams of accelerated electrons and electrostatic or electromagnetic lenses to create images of much higher resolution based on the shorter wavelengths of electrons than visible light photons [36].

In this technique, the electrons are focused to a spot and are scanned successively across the specimen. At each spot, signals are emitted from the specimen and collected by the detectors. The detector signal is synchronized with known location of the beam on the specimen, and the signal intensity is utilized to modulate the corresponding image pixel. Then, these signals are collected in series to originate an image whose dimension/pixel distribution depends on the scan pattern chosen [36].

2.4. Helicobacter pylori

Due to all the properties and biomedical applications of kefiran mentioned above, as well as some studies reporting its impact onto the gastrointestinal health [16], preliminary studies concerning its possible effect on the eradication of *H. pylori* were performed.

2.4.1. Overview

Currently, the percentage of people infected with *Helicobacter pylori* worldwide is estimated at around 50 % [37].

H. pylori is a human gastric pathogenic Gram-negative bacterium, S-shaped, 0.5 x 5 μm in length, with a bunch of 5 to 7 polar sheathed flagella [38, 39]. It is a fastidious microorganism with special nutritional requirements [38, 40] and a microaerophilic organism, requiring less than 5 % of oxygen for growth [41].

This bacterium exhibits various structural and morphological characteristics that stimulate their penetration within the gastric mucosa and thus its colonization. Among the various virulence factors of the *H. pylori*, the main ones are the flagella that enhance their mobility (ability to cross the mucus gel layer and colonize the gastric epithelial cells), urease (enables survival in the gastric environment by buffering the acidic pH in the vicinity of the bacteria), cytotoxin production (damage to gastric cells, such as vacuolation), phospholipase secretion and ability to adhere to target cells (prevents displacement due to peristaltic movements for instance) [37]. *H. pylori* has different strains, which can be classified into two groups: type I, also known as highly virulent, and type II strains that exhibit reduced virulence [42]. This classification depends on the expression of the vacuolating cytotoxin A (VacA) and the cytotoxin-associated gene A (CagA) [43]. Thus, type I strain express both CagA, VacA and infection with these strains is associated with poorer prognosis. Type II strains not only lack the CagA gene but also lack vacuolating activity [44].

A high mutation rate and a high rate of intraspecies genetic recombination are the underlying causes of the high level of genetic diversity among *H. pylori* strains. Furthermore, several populations and subpopulations of this bacterium with different geographic distributions were identified, based on multilocus sequence typing analysis of conserved housekeeping genes [45]. Among the different strains, *H. pylori* J99 and *H.*

pylori 26695 are the most studied and characterized *H. pylori* strains, being these the first ones to be completely sequenced [46].

Morphologically, *H. pylori* may present three morphologies: the bacillary form, the intermediate V- and U-forms and the coccoid form [47]. The process of converting the spiral form to the coccoid form involves passing through the U-shape/V-shape. That is, the growth of the bacteria causes the same to bend and results in a U-shaped bacterium. Finally, the coccoid form is reached when the bacteria reach the "ball-like" form [Figure 6] [48].

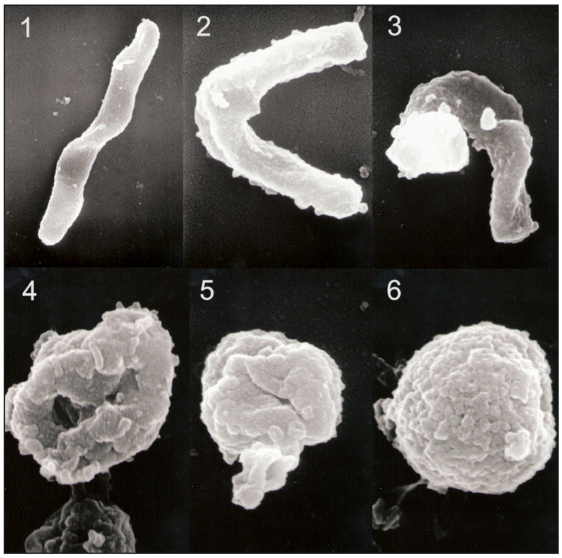

Figure 6. Conversion of *H. pylori* from the bacillary form to the coccoid form. Adapted from [48].

H. pylori acquires the coccoid morphology as a survival strategy when it is exposed to unfavourable conditions, such as nutrient starvation, use of antimicrobial agents, pH of the surrounding environment, changes in oxygen content and media containing growth inhibitors (proton pump inhibitor, bismuth and some antibiotics) [38].

H. pylori is classified since 1994 as a Class I carcinogen. This pathogen does not only induce inflammatory disorders, such as chronic gastritis and ulceration, but it is responsible for 90% of all gastric cancer cases [49]. Gastric cancer is the last step of a precancerous cascade (Correa's cascade) that initiates with (1) *H. pylori* infection of gastric epithelial cells; (2) inflammation of the stomach mucosa (chronic gastritis); (3) loss of stomach cells and weakening of digestive system (atrophic gastritis); (4) transformation of the stomach mucosa (intestinal metaplasia); (5) initial stages of stomach cancer (dysplasia) and; (6) stomach cancer (gastric adenocarcinoma) [Figure 7] [50].

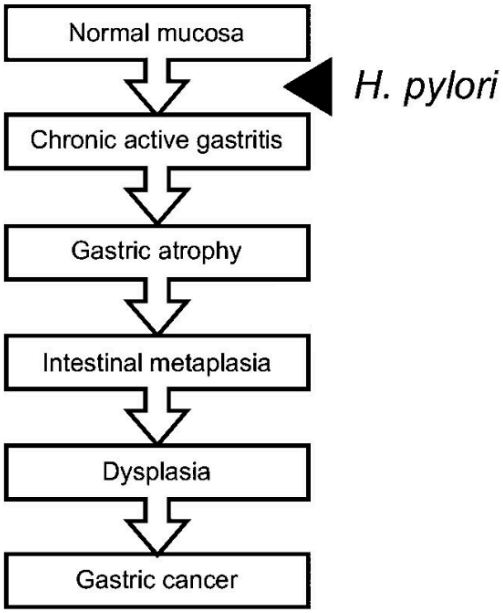

Figure 7. *H. pylori* induced precancerous cascade (Correa's cascade). Adapted from [51].

2.4.2. Infection

Infection with *H. pylori* is usually multistrain and mostly occurs in childhood, affecting both genders [52]. Usually, *H. pylor*i is transmitted through human-to-human, either by faecal-oral or oral-oral route [53]. Oral-oral route seems to be the main way of transmission, which explains the common occurrence of the infection among family members. Thus, the sharing of utensils during meals represents a route of transmission of this bacterium for example. Regarding the faecal-oral route, this happens through the consumption of contaminated water, mainly due to unsatisfactory basic sanitation conditions [54].

Currently, the prevalence of this infection is higher in developing countries compared to developed ones. The prevalence rate varies depending on factors such as ethnicity/race, socioeconomic conditions and age [37]. The occurrence of the infection among middle-aged adults is over 80% in several developing countries, while in industrialized countries it is around 20-50% [55]. Furthermore, the prevalence can differ within a single city and among subgroups within a population [56]. The housing conditions that promote close person-to-person contact, high number of children per household, sharing of beds and lower hygiene are also linked to transmission between family members [53, 57].

A study to evaluate the prevalence of *H. pylori* was performed through a systematic search of articles published between January 1, 2000 and June 31, 2017 and it was possible to estimate the number of infected people through the analysis of 183 papers that reported the prevalence of *H. pylori* in the different countries [Figure 8] [58].

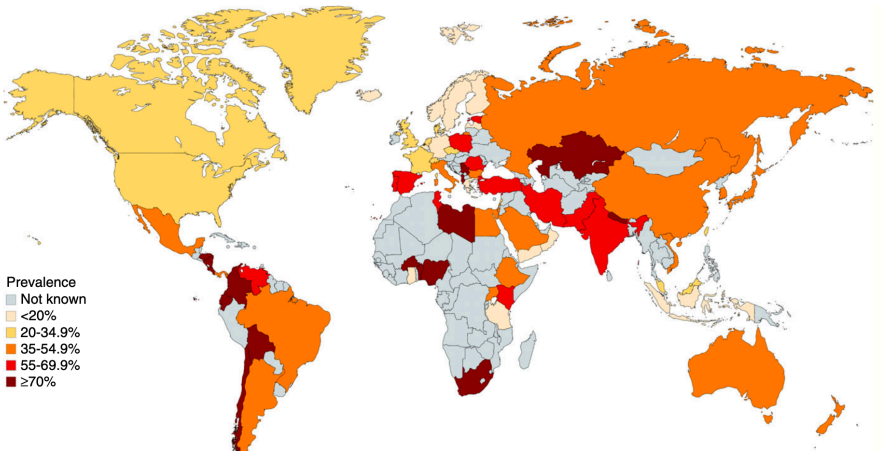

Figure 8. Global prevalence of *H. pylori*. Adapted from [58].

In 2015, approximately 4.4 billion people worldwide were estimated to be positive for *H. pylori*, with an overall global prevalence of this infection set at 44.3% [58, 59]. The percentage of females and males infected is similar [60]. Besides that, when it comes to ethnic groups, the prevalence is 26% in white people and 53% in black people [57].

As far as Portugal is concerned, its *H. pylori* infection rate is one of the highest in Europe [58]. Not long ago, Portugal went through important economic and social changes, namely the transition from a dictatorial regime to a democracy. This change resulted in improvements in the living standards of the Portuguese, however, not all people were covered in the same way. Thus, the rhythm associated with these historical changes allows us to understand the current high prevalence of the infection in the country [61]. Moreover, the Portuguese diet also influences the incidence of infection. This can be explained by the fact that in Portugal, both vegetable soups and sausages are items thar contribute to high sodium consumption. And as such, excessive sodium intake may increase *H. pylori* colonization and exacerbate gastritis, enhancing the carcinogenic process [62].

It is necessary to take into account that this data has some limitations, such as the fact that even though the prevalence is higher in developing countries, there are not many reports available. Moreover, in many countries, data is obtained through willing contributors of population-based studies which underestimates the true prevalence,

especially in areas that have a poorer access to health care facilities. Besides that, since *H. pylori* infection is not a disease usually included in health screening, this results in a reduced chance of identifying the infection in the general population [59].

2.4.3. Virulence factors

H. pylori has several mechanisms that allow its survival in the human stomach, a harsh environment (low pH, gastric cell renewal, shear stress, …). The enzyme urease, produced by *H. pylori*, causes the conversion of urea to ammonia, which allows the acidity of the environment surrounding the bacteria to be neutralized [49]. *H. pylori* also secretes protease, an enzyme that damages the protective mucus layer, which is rich in phospholipid and lipase. This delays the diffusion ability of H^+ ions, increasing the cellular damaging effect due to back diffusion of gastric acid.

H. pylori secretes VacA, which adheres to the surface epithelium with adhesin proteins and originates vacuolization. Through pore formation and apoptosis in mitochondrial membranes, VacA induces host cell death. Furthermore, the oncoprotein CagA is delivered into gastric epithelial cells and interrupts both vesicular trafficking and autophagy pathways [Figure 9] [60].

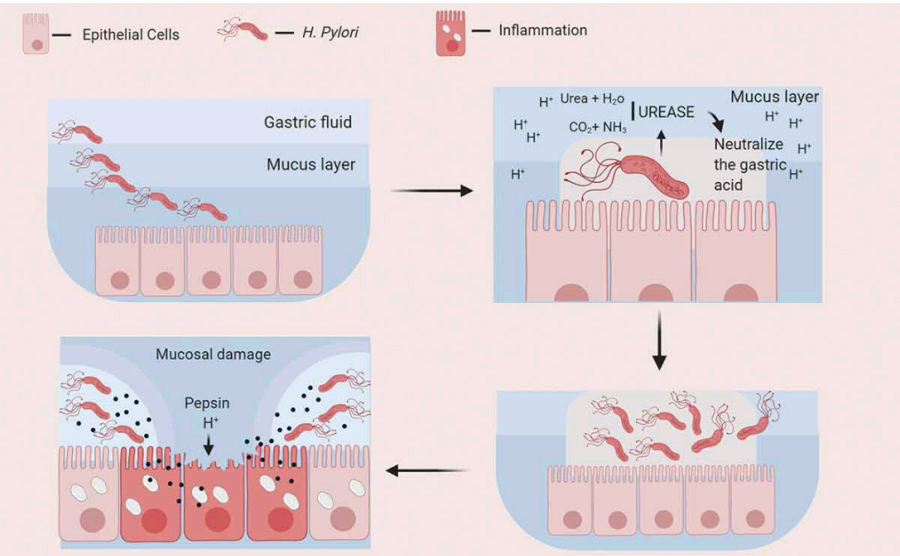

Figure 9. Invasion of *Helicobacter pylori* in the stomach. Adapted from [50].

2.4.1. Diagnosis

H. pylori infection can be confirmed by several methods. The available tests are normally divided into two groups, noninvasive (nonendoscopic) tests, such as stool antigen test, serologic test and urea breath test, and invasive (endoscopic) tests, such as

rapid urease test, histology, culture and polymerase chain reaction, which are equally accurate [51].

Noninvasive methods:

- Stool antigen test: identifies *H. pylori* antigens in the stool through an enzymatic immunoassay or immuno-chromatography [54]. These tests are suitable for follow-up of infection and should be performed after an eight-week period after therapy [55];
- Urea breath test (UBT): urea labelled with 13C or 14C is administrated to patients. If urease is present (due to *H. pylori*), it will convert urea into ammonia and thus, labelled CO_2 will be measured in the exhaled air using a mass or infrared spectrometer [57]. This test is indicated for the early diagnosis of the infection and as follow-up of eradication therapy. In the last case, the test should only be made after a four-week period, to avoid false negative results;
- Serologic tests: used to diagnose *H. pylori* infection in serum, saliva or urine, in patients before treatment [55]. These have been developed through the discovery of specific serological markers [54]. These tests are not appropriate for eradication confirmation, because it does not distinguish between previous and active infections [57].

Invasive methods:

- Endoscopy: is an exam performed to obtain samples for other invasive methods. Uneven distribution of *H. pylori* in the stomach leads to errors in biopsy-based examinations and thus, several attempts have been made for real-time diagnosis of the infection during endoscopic examination [40];
- Rapid urease test (RUT): allows cheap and quick detection of urease activity in the biopsy material extracted with reaction times between 5 minutes and 24 hours [55, 63]. These tests rely on the conversion of urea into ammonia by detecting an increase in the pH of the reagent after adding a biopsy sample containing *H. pylori*. An advantage of this method is that it only detects an active infection [54];
- Histology: provides information on the degree of inflammation and associated pathology, such as metaplasia, dysplasia and malignant neoplasm. The results

obtained can vary due to the number and location of the biopsy samples, the type of stain used and also the experience of the gastroenterologist and pathologist [57];

- Bacterial culture: culture of *H. pylori* from biopsies is based on morphological characteristics as well as biochemical properties, such as positive urease, catalase and oxidase reactions [56, 63]. This method plays a crucial role when a patient presents a failed response to therapy because it allows to perform an antibiotic resistance panel [57];
- Real-time polymerase chain reaction (RT-PCR): allows a fast detection of *H. pylori* with high levels of specificity and sensitivity [56, 63]. This method also allows the characterization of pathogenic genes and antibiotic resistance mutations [63].

2.4.2. Therapeutics

2.4.2.1. Antibiotic-based

There is not an unanimously defined protocol for the treatment of *H. pylori* infection, varying from geographical location to the prescribing physician. The standard eradication treatment involves a combination of antibiotics and acid-suppressive drugs, aiming the eradication of bacteria, regression of symptoms and healing of the damaged mucosa by the infection [41, 54].

Although *H. pylori* is vulnerable to several antibiotics *in vitro*, it is common that they are not effective in infected patients, leading to treatment failure. Failure may be due to inability of antibiotics to achieve effective concentrations in the gastric mucus layer (low bioavailability) and inactivation of antibiotics due to low pH [55]. Moreover, since the infection with this bacterium is multistrain, there is heteroresistance of the different strains to drugs. Consequently, heteroresistant strains may be able to survive in the presence of various antimicrobial drugs [64]. Thus, treatment with only one antibiotic is mostly ineffective [55].

High resistance of *H. pylori*, low bioavailability of antibiotics, difficulty of drugs to reach the site of infection (under the gastric mucosa) and low patient compliance to the therapeutic scheme, mainly due to severe side-effects, led to 20-40% ineffectiveness rates of the recommended antibiotic-based therapy. For instance, clarithromycin is one of the most used antimicrobials against *H. pylori* [65]. However, high prevalence of *H. pylori*

strains resistant to clarithromycin and metronidazole difficult treatment effectiveness. Consequently, rescue line approaches were developed [Table 2] [66].

Table 2. Antibiotic-based approaches to eradicate *Helicobacter pylori*.

Therapy	Description	Length (days)	Reference
First-line (dependent of Clarithromycin resistance)	i) if resistance < 20%: clarithromycin triple therapy; Clarithromycin triple therapy: Proton Pump Inhibitor (PPI), amoxicillin and clarithromycin. Efficiency 70-85%. ii) if resistance > 20%: bismuth quadruple therapy or non-bismuth quadruple therapy: - Bismuth quadruple therapy, it can be recommended as second-line or even first-line therapy. PPIs, bismuth salt, tetracycline and metronidazole. - Non-bismuth quadruple therapies: PPIs, amoxicillin, clarithromycin, metronidazole.	10-14	[37, 56, 67, 68]
Second-line	Bismuth quadruple therapy or levofloxacin triple therapy: PPIs, amoxicillin and levofloxacin.	10-14	[56, 57]
Third-line *	Rifabutin triple therapy (PPI, amoxicillin, rifabutin).	10	[60]

* An antibiotic susceptibility testing (AST) or molecular determination of genotype resistance should be executed before going to third line [60].

2.3.2.2. Non-antibiotic therapeutics (others):

- Probiotics

Probiotics have been implemented in the prevention and treatment of several gastrointestinal infections and therefore, it is believed that these can be useful for the management of the infection caused by *H. pylori*. This is due to: (1) inhibition of *H. pylori* colonization through conquering gastric epithelial receptors or co-aggregation mechanism; (2) anti-*H. pylori* activity throughout the production of bacteriocins, organic acids, as well as biosurfactants; (3) promoting mucin synthesis, (4) modulation of immune system response; (5) induction of antigen-specific antibodies and; (6) decrease of stomach inflammation [68].

Some studies propose that probiotics help in the restoration of the intestinal microbiota disturbed by antibiotics. This leads to a reduction in side effects and, consequently, to an increase in treatment adherence, corroborating the success of the therapy. The benefits of the use of probiotics are associated with immunological and non-immunological mechanisms, such as: (1) competition at the site of the stomach mucosal epithelium; (2) substance production against *H. pylori* such as acetic, propionic or butyric acid; (3) strengthening tight junctions between epithelial cells and; (4) regulation of immune function and secretion of immunoglobulin A to improve mucosal defensive [69].

However, Zagari *et al.* showed that the probiotic supplementation *per se* did not improve the efficacy of the treatment. Thus, the role of probiotics in *H. pylori* eradication is not consolidated and therefore, more studies are required [54].

- Bioengineered strategies

Recently, bioengineering, resourcing to the use of micro- and nanoparticles have been explored to eradicate *H. pylori* infection [50]. For instance, nanotechnology-based drug delivery systems have been developed extensively and accomplished drug protection against acidic and enzyme degradation, pH responsive control release as well as active targeting towards *H. pylori* [70]. When drug encapsulated nanoparticles accumulate in the target site and make sustained release, this can lead to a significant increase in the amount of drug ingested by bacteria [Figure 10] [71].

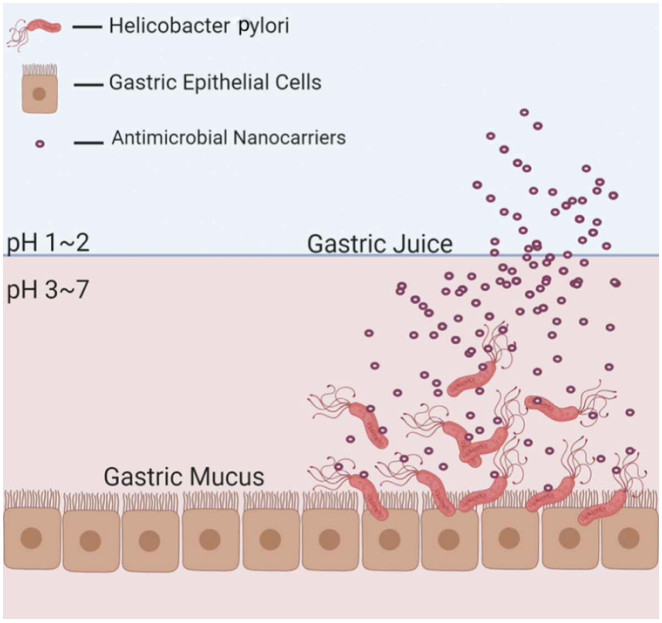

Figure 10. The use of nanoparticles to eradicate *Helicobacter pylori*. Adapted from [50].

Antimicrobial peptides (AMP) are peptides produced by a variety of organisms as a component of innate immunity for protecting the host against pathogens. AMP can kill a variety of pathogens quickly and with high performance levels [72]. Furthermore, these AMP are effective against multidrug-resistant bacteria however, the potential development of bacterial resistance is a major concern [73].

Recently, many efforts have been made to evaluate the efficiency and mechanism of action of the AMP for the treatment of *H. pylori*. Thus, some peptides such as Pexiganan or MSI-78, Tilapia piscidins, Epinecidin-1, Cathelicidins (Human cathelicidin LL-37 and Mouse cathelicidin CRAMP), Defensis (Human neutrophil peptide 1 and SolyC), Bicarinalin, Odorranain-HP, PLGa-AM1, Bacteriocins (Pediocin BA28 and Bulgaricin BB18) have demonstrated antimicrobial action against *H. pylori* [72].

Several nanoparticles, composed of different types of materials such as metals, polymers, magnetics and lipids have been developed with the aim of eradicating this infection [37].

Metallic nanoparticles are mainly composed by pure metal precursors, which possess unique optoelectrical features because of their localized surface plasmon resonance (LSPR) characteristics. Gold, zinc, silver and bismuth are some of the elements that make up the metallic nanoparticles. Saravanakumar *et al.* synthetized silver nanoparticles from the aqueous bark extract of *Toxicodendron vernicifluum* and these exhibited antibacterial potential against *H. pylori* by inducing the production of reactive

oxygen species, oxidative stress, nucleus damage, DNA division and apoptosis in *H. pylori* cells [74]. Gopinath *et al.* developed gold particles from fruit extract of *Tribulus terrestris*, which exhibited antibacterial activity against multi-drug resistant clinical strains of the bacterium. Moreover, these nanoparticles did not show cytotoxic effects against human gastric adenocarcinoma (AGS) cells [75].

Polymeric nanoparticles are organic and can present nano-spherical or nano-capsular shapes [50]. Polymeric carbohydrate molecules are called polysaccharides, such as alginate and chitosan [37]. Chitosan possesses antibacterial properties and can be useful when conjugated with linoleic acid. Cong *et al.* produced a polymeric nano-micelle in which carboxymethyl chitosan was hydrophobically altered with stearic acid and the obtained co-polymer was then conjugated with urea. These co-polymers had no cytotoxicity against AGS cells, the retention time in the stomach was close to 24 hours and had significant anti-*H. pylori* activity [70].

Lipid nanoparticles are made of lipid moieties with a spherical diameter. They consist of a solid lipid core and a matrix containing soluble lipophilic molecules, being the external core stabilized with emulsifiers and surfactants [50]. Sharaf *et al.* developed nanostructured lipid carriers loaded with hesperidin and clarithromycin. The *in vitro* results obtained showed that the nanoparticles interacted with *H. pylori* through adhesion to the outer cell membrane, resulting in the disruption of the membrane and leakage of cytoplasmic contents. Moreover, it was also observed that the nanoparticles were nontoxic to human cells [66].

Magnetic nanoparticles are also recognized to possess strong antibacterial properties. Sharaf *et al.* developed rod-shaped iron oxide nanoparticles by using ferric chloride with water extract of *Spirulina platensis*. These were then tested against multi-drug resistant *H. pylori* and the results showed that the cell membrane was disrupted and the bacterial compounds from *H. pylori* were leaked, with no adverse effects on human epithelial cells [76].

- Vaccines

A promising alternative may be the development of vaccines. Recently, studies with the aim of developing reverse vaccines with the help of bioinformatics and five antigenic epitopes have been explored as potential vaccine candidates namely, babA,

sabA, fecA, vacA and omp16. Despite that, their development has been a major challenge since it has not been successful in experimental models.

In 2015, a randomized phase 3 study with children has been conducted in China using oral vaccines with recombinant B urease. The sustained vaccine protection against *H. pylori* infection up to 3 years suggests that it could substantially reduce infection. However, longer follow-up in the vaccinated people should be warranted to provide direct evidence of the vaccine efficacy against *H. pylori*-associated diseases [54]. Since there is no effective vaccine, management of *H. pylori* infection still is the main strategy to reduce the spread of the bacterium in the population and prevent the subsequent development of gastric cancer [64].

- Natural compounds

Natural compounds emerged as a good option to fight this bacterium. A variety of plant-based compounds have bactericidal properties against *H. pylori*, such as flavonoids, polyphenols, quinones, terpenoids, coumarins and alkaloids. Furthermore, tea products, garlic extract, ginger-root extracts, quercetin, apple peel polyphenols and others have the capacity of inhibiting bacterial adhesion to the gastric mucosa and also decreasing free radicals. *In vitro* and *in vivo* studies have been performed to establish their mechanism of action [50]. As an example, medicinal plants such as *Zingiber officinalis*, *Korean red ginseng*, *Cistus laurifolius*, *Allium sativum* are described to supress *H. pylori* colonization and reduce gastric inflammation through chemokine release, inhibition of cytokines as well as suppressing precancerous alterations by suppressing nuclear factor-kappa B DNA binding, which suppresses mutagenesis and produces abundant levels of apoptosis [67].

2.5. Polymeric nanoparticles production

Different techniques can be applied to develop polymeric nanoparticles, which include emulsification, solvent extraction, nanoprecipitation, among others [77]. Regarding nanoprecipitation, this technique comprises the traditional nanoprecipitation, flash nanoprecipitation and microfluidic-based nanoprecipitation [78].

In the traditional nanoprecipitation, the polymer is dissolved in a water-miscible solvent and then, this solution is added dropwise into an aqueous solution under stirring. Due to fast spontaneous diffusion of the polymer solution into the aqueous phase, the nanoparticles form immediately to avoid the water molecules. This technique is usually

implemented for encapsulation of hydrophobic or hydrophilic compounds as well as natural compounds [79].

Microfluidic-based nanoprecipitation methods have enormous potential to synthetize nanoparticles with narrow size distribution, distinct shapes and allow superior control over the process of nanoprecipitation. A microfluidic system has a microfluidic chip that contains a pattern of microchannels, which are either moulded or engraved. These pathways allow fluids to be injected and evacuated from the microfluidic chip [80].

Another technique for particle production is the ionotropic gelation. This technique is a physicochemical process of microdroplet hardening that allows the production of nanoparticles (NP) and microparticles. This occurs through electrostatic interactions between two ionic species under certain conditions, where at least one of the species needs to be a polymer [81, 82].

CHAPTER 3 – MATERIALS AND METHODS

3. Materials and Methods

3.1. Kefiran production

The protocol used throughout the present work to prepare the kefiran was adapted from the ones described in the literature [13]. First, kefir grains from a home culture [Figure 11 A] were added in a 1:10 ratio to Type II water (deionized water) heated at 80 ºC for 1h and under magnetic stirring [83]. Then the solution was centrifuged (Eppendorf 5810R) for 20 minutes at 20 ºC at 4000 revolutions per minute (rpm). The pellet was discarded and the supernatant was then added to 96% (v/v) ethanol (aga) in a 1:2 ratio and left overnight at room temperature (RT) [Figure 11 B].

Afterwards, the solution was centrifuged again for 20 minutes at 20 ºC at 4000 rpm. The resulting precipitate [Figure 11 C] was heated at 80 ºC for 1 hour with Type II water in a 1:10 ratio. Then, the resulting solution was added to 96% ethanol (aga) in a 1:2 ratio and left overnight at RT. Finally, the precipitate was dried in an oven at 60 ºC overnight, thus yielding kefiran [Figure 11 D].

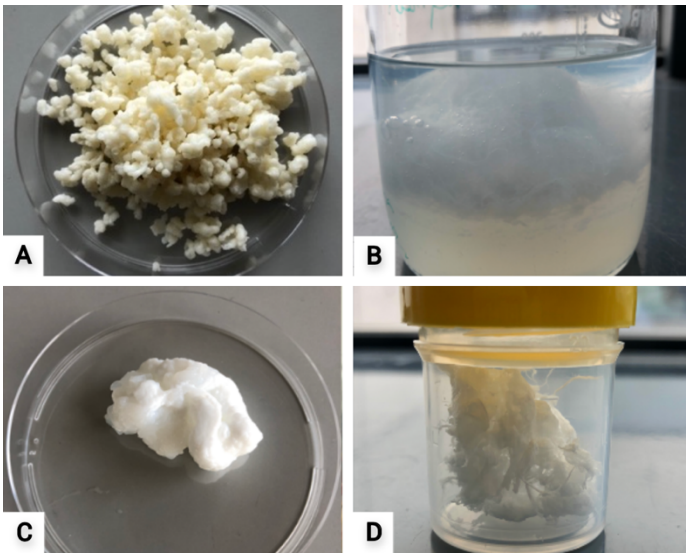

Figure 11. (A) Kefir grains, (B) Precipitation process, (C) Precipitate formed and (D) Kefiran.

3.2. Kefiran characterisation

3.2.1. Fourier-Transform Infrared Spectroscopy (FTIR)

Fourier-Transform Infrared Spectroscopy (FTIR) analysis was carried out on a Perkin-Elmer System 2000 FTIR spectrometer. Spectra were recorded in the spectral

range of 4000 cm^{-1} to 400 cm^{-1} at 4 cm^{-1} spectral resolution, and 200 sample/background scans using Perkin Elmer Spectrum Software (v10.5.2).

3.2.2. Confocal Raman Microscopy (CRM)

For Confocal Raman Microscopy (CRM) analysis, a Raman spectrometer HORIBA JOBIN YVON HR800 UV connected to LabSpec software was used. Each analysis involved 2 scans, 120 sec of acquisition, a green laser with 515.2 nm wavelength and a confocal hole of 100 μm. Before each analysis, the equipment was calibrated using silicon.

To increase the signal intensity, the sample to be observed was placed on aluminium foil covering a glass slide. A drop of distilled water was poured into the sample in order to guarantee its adherence to the aluminium foil, being the excess of water removed with paper by capillarity.

3.2.3. Differential Scanning Calorimetry (DSC) and Thermogravimetric Analysis (TGA)

DSC and TGA analyses were performed using the thermal analyser NETZSCH STA 449F3. The sample was placed in aluminium crucibles and subjected to heating from 235 °C to 500 °C at a rate of 10 K/min, under an atmosphere of nitrogen at a rate of 50 mL/min.

3.2.4. Zeta Potential (ZP)

Zeta potential (ZP) of samples were determined from streaming potential measurements with a commercial electrokinetic analyser (EKA) (Anton Paar GmbH, Austria) using a special powder cell adapted inside a cylindrical cell, used for particles analysis. Kefiran was mounted inside the powder cell occupying a volume of roughly 48,75 mm^3, thus maintaining an overall constant height of sample for all the measurements.

Streaming potential was measured using Ag/AgCl electrodes installed at both ends of the streaming channel, the cylindrical cell. The electrolyte used was 1 mM KCl (potassium chloride) with the pH value varying between 8 and 9. Experiments were performed around 26 °C. The conductivity of the electrolyte solution was measured during the assay. The streaming potential was measured while applying an electrolyte

flow in alternating directions and pressure ramps from 0 to 200 mbar. For each sample, 12 pressure ramps were performed, 6 in each flow direction in order to cope with the asymmetric potential fluctuations.

3.3. Kefiran/alginate microparticles preparation

Taking advantage of the fact that alginate can be crosslinked in the presence of multivalent cations such as Ca^{2+}, hybrid kefiran/alginate nanoparticles were prepared (section 3.4) to be used in *in vitro* cells and bacteria tests. Previously to the nanoparticles preparation, different w/v ratios of kefiran/alginate mixtures were tested, and microparticles prepared [Table3].

Table 3. Different w/v ratios of kefiran/alginate mixtures.

	Kefiran (2% w/v) Alginate (1% w/v)	**Kefiran (2% w/v) Alginate (2% w/v)**
	Kefiran/Alginate ratio	**Kefiran/Alginate ratio**
Sol. A	90/10	90/10
Sol. B	80/20	80/20
Sol. C	66/33	70/30
Sol. D	50/50	50/50

Kefiran solution (2% w/v) was prepared using Type II water. An initial attempt was made to produce the solution by magnetic stirring at RT. However, it was visible to the naked eye that the kefiran did not completely dissolve. As such, kefiran solutions were prepared in a water bath at 40 ºC for 10 minutes. This protocol generated a homogeneous kefiran solution.

Concerning the alginate (ultra-pure sodium alginate with high content of guluronic acid units (>60%, NovaMatrix, FMC Biopolymers), molecular weight of 131 $\pm$ 13 kDa) a 1% w/v and 2% w/v solutions were prepared by adding the alginate to Type II water. Magnetic stirring was applied for 10 minutes so that the resulting solution was homogeneous.

For the preparation of the microparticles, the different kefiran/alginate formulations were manually dropwise extruded, using a syringe (∅ = 4.68 mm) with a needle (20G) at the tip, into a 0.1 M calcium chloride (Merck KGaA) solution.

3.4. Kefiran/alginate nanoparticles (Kef/Alg NP) preparation and characterisation

3.4.1. Nanoparticles preparation

The droplet extrusion method combined with ionotropic gelation in the presence of Ca^{2+} was also used in the preparation of the nanoparticles, following two different approaches, namely, extrusion of kefiran/alginate solution directly through a syringe needle (20G), and using a microfluidic device. In both situations, a syringe pump (NE-1000) with a flow rate of 0.5 mL/min, was used as well as a 0.1 M $CaCl_2$ crosslinking solution. The particles produced were left overnight in agitation (750 rpm) at RT [Figure 12].

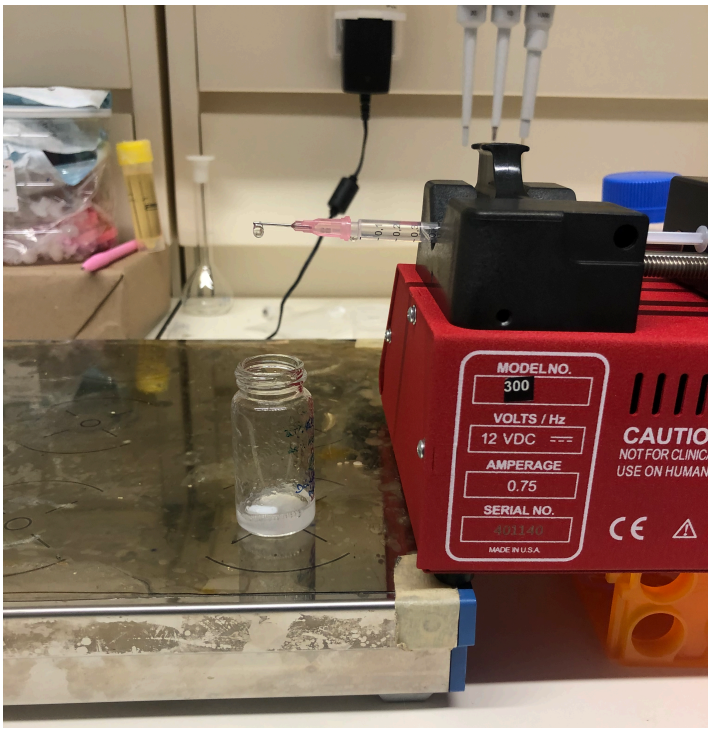

Figure 12. Setup for the ionotropic gelation technique.

Also, a microfluidic setup using two syringes was implemented [Figure 13]. One of the syringes (∅ = 4.68 mm) had the kefiran/alginate solution and the other one (∅ = 12.07 mm) was filled with calcium chloride solution, each syringe being placed in a syringe pump (NE-1000). The gel drops fell into Type I water (Milli-Q® water). Flow

rates of 1 µL/min and 10 µL/min were used for the kefiran/alginate and calcium chloride solutions, respectively.

Finally, the previous setup was modified by using Type I water in one of the syringes and kefiran/alginate solution in the other one, nanoparticles felling into the calcium chloride solution. The nanoparticles produced were left overnight at 70 rpm at RT [Figure 13].

Figure 13. Setup for the microfluidic system.

Kefiran/alginate nanoparticles incorporating the MSI-78 (Pexiganan) peptide, in a concentration of 2 mg/mL were also prepared using the setup previously described.

3.4.2. Nanoparticle Tracking Analysis (NTA)

For the Nanoparticle Tracking Analysis (NTA), the samples were composed by 10 µL of nanoparticles and 990 µL of Type I water (Milli-Q® water), a dilution of 1:100. Then to analyse the samples, the NanoSight NS300 particles counter, RRID:SCR_014239 was used, in order to evaluate the concentration and size of the nanoparticles.

3.4.3. Nanoparticle peptide release

The amount of MSI-78 released from the nanoparticles was calculated by UV/Vis spectrophotometry (Lambda 45; Perkin Elmer), based on the concentration of MSI-78 on the supernatant. Released MSI-78 concentrations were calculated using a calibration curve, previously prepared by measuring decreasing AMP concentrations from 500 to

32.5 μg/mL, at a wavelength of 205 nm as described previously [84]. NP were incubated in PBS (Phosphate-Buffered Saline) for 2 h, 24 h and 48 h, at 150 rpm and 37 ºC. In each timepoint, AMP released from the nanoparticles was determined by the difference between the initial amount of MSI-78 (2 mg/mL) and the quantity of released AMP present on the supernatant. EDTA (Ethylenediaminetetraacetic acid) was used as positive control since it breaks the crosslinking and, consequently, leads to the disruption of the nanoparticles (*i.e.*, all the AMP encapsulated is released) [85].

3.5.*In vitro* tests

3.5.1. Bacteria tests

3.5.1.1. Helicobacter pylori

Two *H. pylori* strains, *H. pylori* J99 and *H. pylori* 26695 (provided by Department of Medical Biochemistry and Biophysics, Umeå University, Sweden) were cultured as described [86]. Briefly, *H. pylori* was cultured in Blood Agar (BA; Oxoid, France) supplemented with 10% of defibrinated horse blood (Probiologica, Portugal) and with an antibiotic cocktail (polymyxin B, vancomycin, amphotericin B, trimethoprim; all supplied by Sigma-Aldrich) under microaerophilic conditions (<5% O_2; GenBox System, BioMérieux) at 37 ºC for 48 h. Then, a few colonies were streaked onto fresh BA medium and incubated under the same conditions for another 48 h. A pre-inoculum of *H. pylori* was prepared by harvesting the bacteria spread from the agar plates with Brucella Broth (BB) supplemented with 10% of inactivated Fetal Bovine Serum (FBS, Gibco^{TM}) (BB + 10% (v/v) FBS). After this, the bacterium was adjusted to an optical density (OD) of 0.1 (λ=600 nm; approximately 1x10^9 CFU/mL) in BB+10% FBS, placed in a T-flask and incubated overnight (16h-18h) at 37 ºC, 150 rpm. Afterwards, bacterial inoculum was adjusted to 0.03 optical density at 600 nm (OD_{600}), which corresponds to approximately 1 x 10^7 colony forming units (CFUs)/mL [87]. This concentration was used in all the subsequent bacterial assays. The initial inoculum concentration was confirmed by serial dilution in PBS of the bacterial suspension and inoculation of 20 μL drops onto BA. The number of colony forming units (CFUs) were counted after 5 days of incubation [Figure 14] in the same above-mentioned settings and the number of CFUs/mL were determined.

The *H. pylori* culture adjusted to 1 x 10^7 CFU/mL was added to a 96-well plate (Starsted) and incubated with different concentrations of the designed nanoparticles (10^9,

10^8 and 10^7 particle/mL) in culture medium over 24h, at 150 rpm, 37 ºC, under microaerophilic environment.

Afterwards, serial dilution in PBS was performed (up to 10^7) and 20 µL drops were plated in triplicate per dilution [Figure 14]. After five days of incubation, at 37 ºC and under microaerophilic conditions, the CFUs/mL were determined.

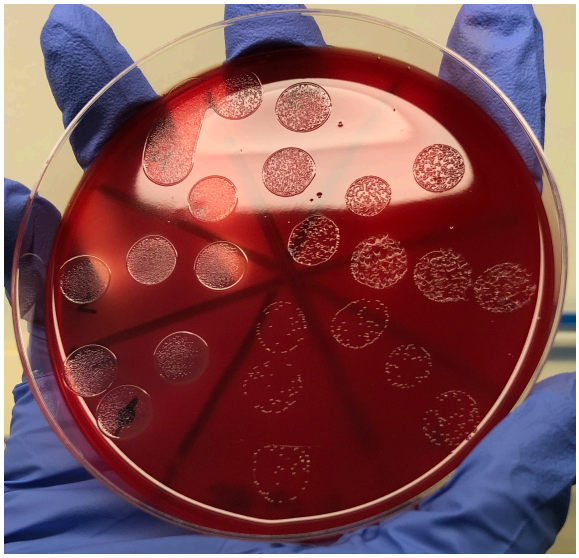

Figure 14. *H. pylori* after 5 days of incubation.

Two independent assays were performed with duplicates and results are expressed as mean with standard deviation.

3.5.1.2. *Escherichia coli* and *Lactobacillus acidophilus*

Escherichia coli (ATCC 25922®, American Type Culture Collection, Manassas, VA, USA) was cultured as described [88]. In short, *E. coli* was streaked and cultured in Tryptic Soy Agar (TSA; Merck, Germany) under aerobic conditions at 37 ºC overnight. Afterwards, a colony was selected and incubated onto Tryptic Soy Broth (TSB, Merck, Germany) at 37 ºC, 150 rpm, overnight. Bacterial inoculum was then adjusted to 1 x 10^5 colony forming units (CFUs)/mL by reading the OD at 600 nm (OD_{600}) as described [89]. The initial inoculum concentration was confirmed by serial dilution and plating of 10 µL drops of the bacterial suspension onto TSA via drop plate method. Finally, CFUs were counted after 24 h of incubation in the same above-mentioned settings and CFUs/mL calculated.

Lactobacillus acidophilus-05 (LA-5®, provided by Chr. Hansen, Hørsholm Denmark) was cultured as described [88]. Shortly, *L. acidophilus* was cultured in De

Man-Rogosa and Sharpe Agar (MRS; Biokar, France) under microaerophilic conditions (plate was sealed with parafilm) at 37 ºC for 24 h. Then, *L. acidophilus* was harvest and incubated in MRS brucella broth (Biokar Diagnostics) at 37 ºC, 150 rpm, overnight, in a microaerophilic environment. Bacterial inoculum was adjusted to 1 x 10^5 colony forming units (CFUs)/mL after reading the OD at 600 nm (OD_{600}) [89]. The initial inoculum was confirmed as described for *E. coli*.

E. coli and L. acidophilus cultures adjusted to 1 x 10^5 CFU/mL were placed in a 96-well plate (Starsted) and incubated with different concentrations of the designed nanoparticles (10^9, 10^8 and 10^7 particle/mL) in either PBS or culture medium over 2h, at 150 rpm, 37ºC.

Afterwards, serial dilution in PBS was performed (up to 10^7) and 10 µL drops were plated via drop plate method in the respective culture medium. *E. coli* CFUs/mL were determined after 24 h of incubation at 37ºC, while *L. acidophilus* CFUs were counted after 48h [Figure 15].

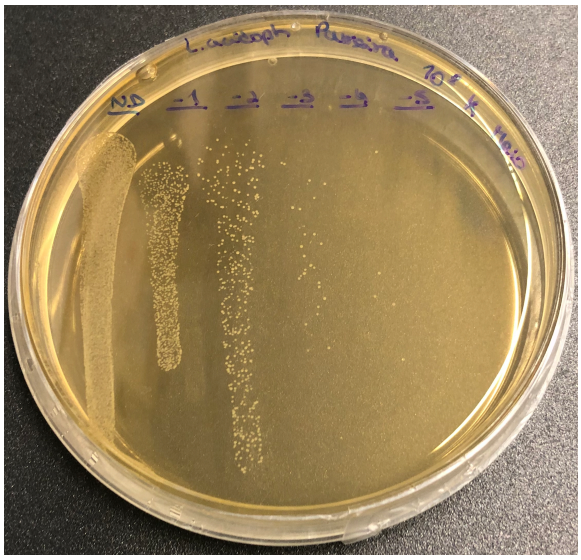

Figure 15. *Lactobacillus acidophilus*-05 after 24h incubation.

Two independent assays were performed with duplicates and results are expressed as mean with standard deviation.

3.5.2. Kefiran cytotoxicity tests

Kefiran cytotoxicity towards a human gastric adenocarcinoma cell line (AGS, ATCC® CRL-1739™) was analysed through direct contact assays, according to the international standard ISO 10993-5;12 [90].

AGS cells were grown in RPMI complete medium, consisting of RPMI 1640 medium with glutamax (Gibco, Invitrogen), supplemented with 10% heat inactivated (30 min, 56 ºC) fetal bovine serum (FBS, Gibco), 10 U/mL penicillin (Biowest) and 10 μg/mL streptomycin (Biowest) at 37 ºC in a humidified atmosphere of 5% CO_2. Afterwards, cells were seeded in 96-well plates (1 x 10^4 cells per well), for the direct contact assay, under the conditions mentioned above. A positive control for non-cytotoxicity was established with cells alone and a negative control was achieved by adding a solution 10% (v/v) of hydrogen peroxide ($H_2O_2$30V; Merck) to the cells.

After 24 hours of cell seeding, culture medium was replaced with a 2% (w/v) kefiran solution in cell culture media. After 24 h incubation, the resazurin assay was performed to evaluate cell metabolic activity. For that, resazurin (20% v/v) was added to the wells and incubated for 4 h. Then, 100 μL of supernatant was transferred to black 96-well plates and fluorescence measured (λ_{ex} = 530 nm, λ_{em} = 590 nm) in a microplate fluorometer (Spectra Max GeminiXS, Molecular Devices). Blanks for fluorescence emission subtraction were performed with only complete culture medium and kefiran without cells.

Cell viability was determined through the average of three replicates, being exhibited as the percentage of the metabolic activity of treated cells in relation to cells in culture medium alone (eq.1).

$$\%\ \text{Cell metabolic activity} = \frac{F_{exp} - F_{blank}}{F_{control} - F_{blank}} \times 100 \quad \text{(eq.1)}$$

Two independent assays with duplicates per condition were done and results are expressed as mean with standard deviation.

3.5.3. 3.7 Statistical analysis

Unpaired t-test with a 95% confidence interval ($p<0.05$) were used to assess statistical significance using GraphPad Prism 9 (9.2.0).

3.6. Kefiran discs preparation and characterisation

3.6.1. Kefiran discs preparation

Having in mind the possibility of using kefiran as porous scaffolds for tissue engineering applications, kefiran discs were prepared using a 2% w/v kefiran solution and

the freeze-drying technique, a process in which a completely frozen sample is placed under a vacuum in order to remove water or other solvents from the sample, allowing the ice to change directly from a solid to a vapor, without passing through a liquid phase. Kefiran solution viscosity was evaluated using a rheometer (Kinexus Pro, Malvern Instruments Ltd, UK). A cone-plate system (upper geometry CP 4/40 SR0041 SS and lower geometry PLS55 C0127 SS) was used. The measurements were performed by varying the shear rates (0,1-1000 s^{-1}) at 25 °C (Peltier system).

Discs were prepared in a 48-well plate (SPL Life Sciences) by depositing 500 µL of the 2% w/v kefiran solution in each well. The plate was kept in the freezer at -20 ºC overnight. After that, the plate was covered with parafilm, perforated in order to allow vapour release and placed in the lyophilizer (FreeZone 2,5 L Freeze Dryer, Labconco) overnight.

3.6.2. Kefiran discs characterization

3.6.2.1. Scanning Electron Microscopy (SEM)

SEM examination of the discs was performed using a tabletop scanning electron microscope with energy-dispersive X-ray spectroscopy analysis module (Hitachi TM4000/Bruker Quantax75) at 20 kV, with secondary electron detector. Images at 60x, 250x and 500x magnification were taken, without any coating.

3.6.2.2. Rheology tests

The rheological properties of kefiran discs were determined using a Kinexus Pro rheometer (Malvern Instruments, Malvern, UK), at 25 °C in a water-vapor saturated environment ensured by the rheometer chamber. For the oscillatory measurements, parallel plate geometries were used. The linear viscoelastic region of the samples was determined using Ø 8 mm sandblasted parallel plate geometries, compressing the samples (oscillatory measurement gap), and iteratively performing strain amplitude sweep and frequency sweep measurements.

The strain amplitude sweeps were performed between 0,01 to 100%, with a fixed frequency of 1 Hz. The frequency sweeps were performed over a range between 0,01 to 100 Hz, at a fixed shear strain of 1%.

CHAPTER 4 – RESULTS AND DISCUSSION

4. Results and Discussion

4.1. Kefiran characterisation

4.1.1. Fourier-Transform Infrared Spectroscopy (FTIR)

In order to chemically characterize the produced kefiran, FTIR analysis was performed. The obtained FTIR spectrum had its baseline corrected using the Spectragryph software, version 1.2.15. The spectrum obtained from the analysis is shown in Figure 16.

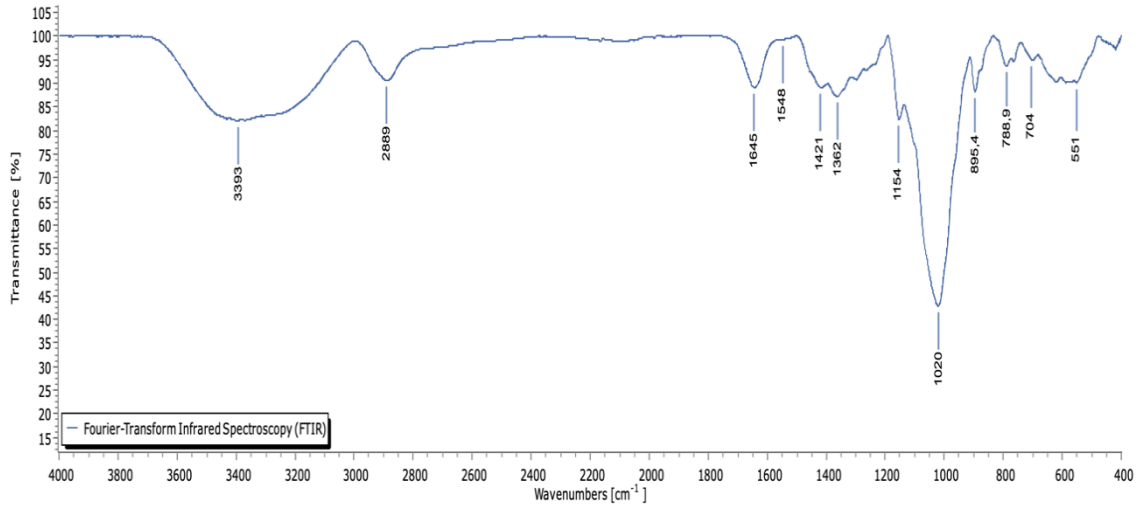

Figure 16. FTIR spectrum of kefiran produced.

According to the literature, the bands correspond to the functional groups and chemical bonds of the exopolysaccharide kefiran [91]. The band at 3393 cm^{-1} corresponds to the hydroxyl groups of the kefiran produced, this region of the band being attributed to the O-H stretching vibration in the constituent sugar residues. The 2889 cm^{-1} band is associated with the stretching vibration of C-H in the sugar ring and can be attributed to methyl (CH_3) and methylene (CH_2) groups. The 1645 cm^{-1} band occurs due to the O-H stretching vibration. Then, the 1421 cm^{-1} band is assigned to the CH_2 and OH groups. The region between 1100 cm^{-1} and 1150 cm^{-1} presents intense absorption, which is a characteristic of the C-O-C stretches and alcohol groups in carbohydrates. As for the 895.4 cm^{-1} band, it indicates the presence of β-glycosidic linkages.

One advantage of kefiran is having nisin, an antibacterial lantibiotic in its composition. The lantibiotics are a group of ribosomally synthesised, post-translationally modified peptides containing unusual amino acids, such as dehydrated and lanthionine residues [92]. According to what is described in the literature, pure nisin FTIR spectra

shows broad bands at around 3270 cm^{-1} due to the OH stretching of COOH group, a peak at 2974 cm^{-1} which is assigned to C–H stretching, and more peaks at around amide I (1620 cm^{-1}, stretching vibration of C=O bond), and amide II (1570 cm^{-1}, bending vibration of the N–H bond) bands [93, 94]. FTIR results showed that most of the pure nisin functional groups could be observed in kefiran spectrum. Further studies should be performed in order to confirm nisin presence.

Comparing the practical results obtained with the theorical values described in the literature, it is possible to infer that they are similar, although the wavelength values of the peaks are not exactly the same. These differences may be related to the production method used [6].

4.1.2. Confocal Raman Microscopy (CRM)

Subsequently, the CRM technique was used to characterise the kefiran produced. The spectrum obtained is shown in Figure 17.

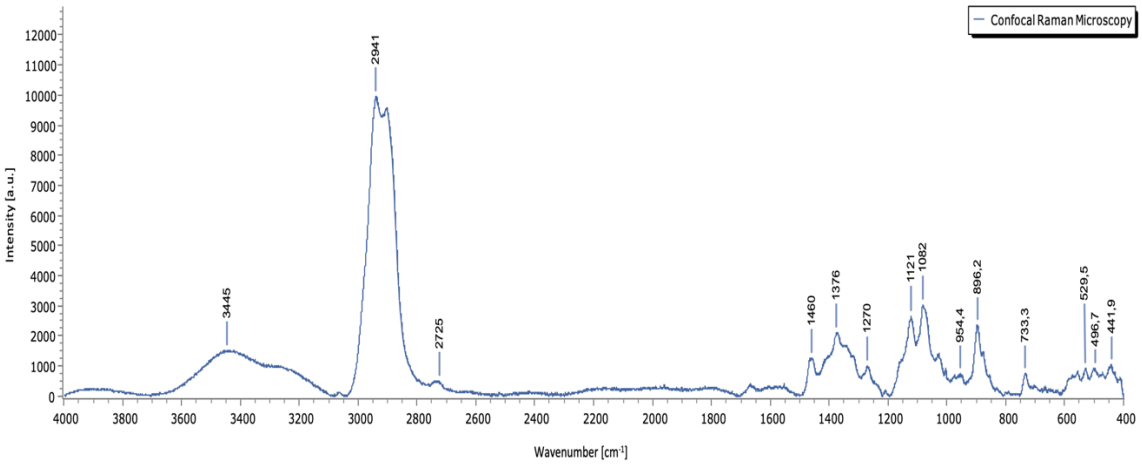

Figure 17. CRM spectrum of kefiran produced.

Based on the Confocal Raman Microscopy band assignments, it can be seen that the chemical information in kefiran is mainly due to the saccharides [95]. Its specific bands centred in the vicinity of 3445 cm^{-1} correspond to O-H stretching vibration mode. The peaks at 2941 cm^{-1} and 2725 cm^{-1} are associated to C-H stretching vibration. The band at 1460 cm^{-1} is characteristic of O-H deformation vibration. In the fingerprinting region it can be observed the scattering bands attributed to CH_2 group deformation vibration in the vicinity of 1460 and 1376 cm^{-1}, the deformation vibration of C-C-H, O-C-H, and C-O-H in the vicinity of 1270 cm^{-1} and the C-O-H group deformation vibration at 1121 cm^{-1}. The region of 1082 cm^{-1} can be assigned to the ring vibrations overlapped

with stretching vibrations (C-OH) side groups and (C-O-C) glycosidic band vibration, which are characteristic of polysaccharides. The 896.2 cm^{-1} band indicates the presence of β-glycosidic linkages and ring deformation vibration in the vicinity of 630 cm^{-1}. Scattering bands observed in the 400 and 600 cm^{-1} regions are attributed mainly the skeletal vibrational motions with major contributions from the deformation modes of C-C-C, C-C-O, C-C, and C-O groups of saccharides [96].

Zimet *et al.* characterized nisin by Raman spectroscopy and the nisin Raman spectra revealed characteristic bands of peptides and proteins, with vibrational modes of amide I at 1676 cm^{-1}, amide III at 1245 cm^{-1}, C-H stretching of aliphatic residues at 2880, 2935, and 2980 cm^{-1}, C-S stretch at 625 and 648 cm^{-1}, C-S stretch trans conformation at 700, 720 and 741 cm^{-1} and anti-symmetric deformations of peptide side chains at 1425, 1450 and 1475 cm^{-1} [97-99]. Most of these bands are also present in the Confocal Raman spectrum of kefiran, supporting nisin presence in the polymer.

4.1.1. Thermogravimetric Analysis (TGA) and Differential Scanning Calorimetry (DSC)

The thermal characteristics of polysaccharides, such as the absorption and emission energies, are accompanied by physical changes, including the structural deformation or melting of the crystalline polysaccharide [100]. A TGA and DSC analysis was performed on the kefiran produced and the thermograms obtained are shown in Figure 18 and Figure 19.

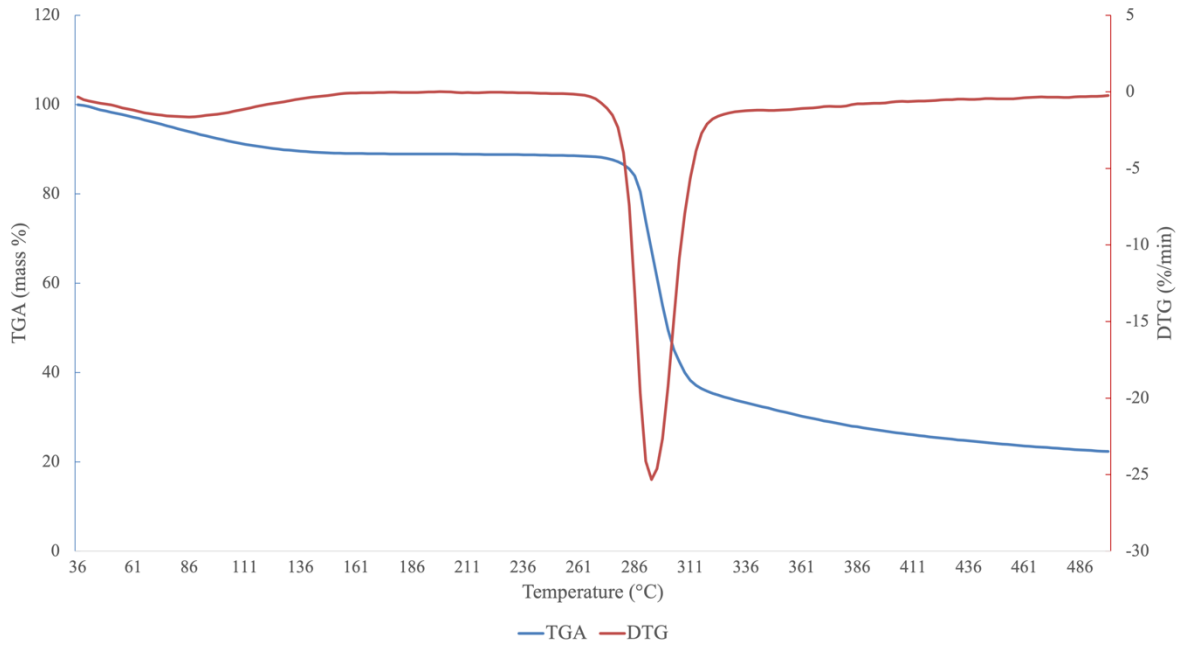

Figure 18. TGA and DTG thermogram of kefiran produced.

With increasing temperature, two events were observed in the TGA kefiran curve. The first one occurred between 36 ºC and 130 ºC with the maximum mass decrease (approximately 10%) occurring at 110 ºC. This can be due to the loss of moisture present in the sample. At 280 ºC an endothermic reaction occurs with energy consumption, possibly due to melting. From 280 ºC upward, kefiran releases energy that is represented by an exothermic peak with a maximum at 310 ºC [Figure 19], indicating a degradation of the polymer. At this point, a large mass loss (60% of the initial mass) can be observed till the temperature of 311 ºC. Then the mass gradually decreases till 500 ºC until 22% of the original mass remained.

In Figure 18, Derivative Thermogravimetry (DTG) curve is also represented showing that an abrupt mass variation occurs at the interval between 270 ºC and 311 ºC.

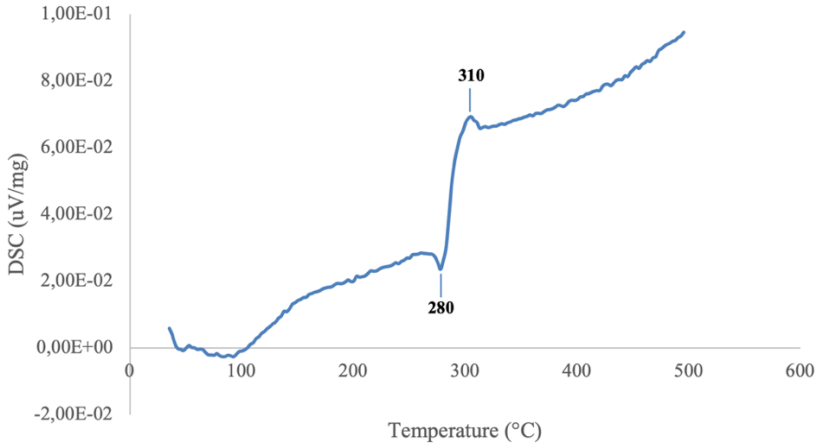

Figure 19. DSC thermogram of kefiran produced.

4.1.2. Zeta Potential (ZP)

ZP analysis involved performing 12 pressure ramps, where the average pH of the 1 mM KCl solution was 8.676846. Regarding the ZP value, the average value obtained was -3.21962 mV.

In general, ZP values between -10 and 10 mV are considered nearly neutral. Values more positive than +30 mV or more negative than -30 mV are usually labeled as stable and, strongly cationic and anionic, respectively [101].

Thus, analyzing the value obtained from the ZP analysis of kefiran, it is possible to verify that it is in the range of values considered neutral. That is, kefiran is in charge balance, having the same number of cations and protons in its composition.

4.1.3. Rheology

Finally, the rheology of the kefiran solution (2% w/v) was analysed. The viscosity curve with the shear viscosity as a function to the shear rate is shown in Figure 20.

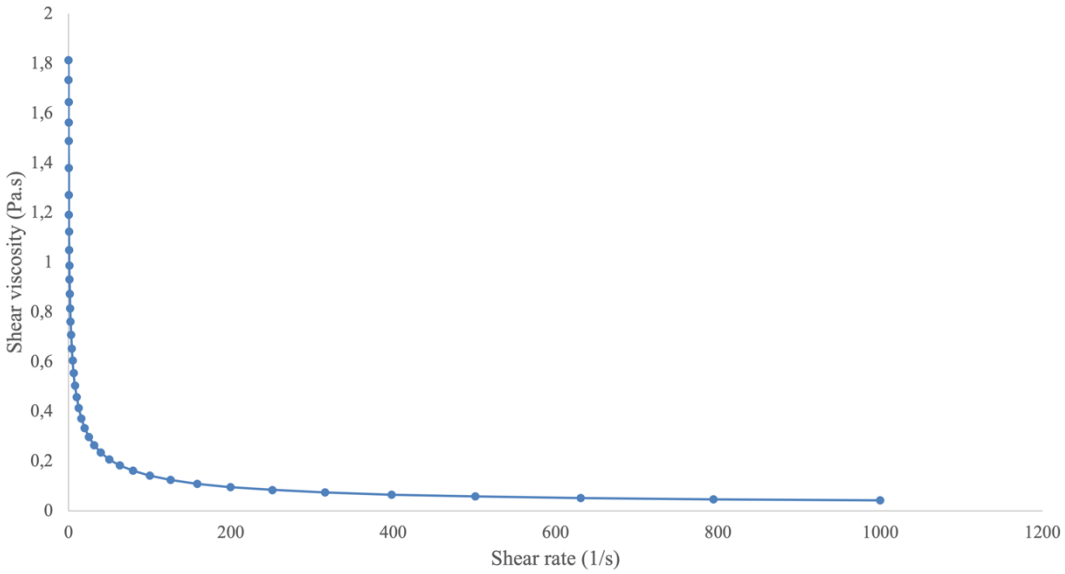

Figure 20. Shear viscosity curve of kefiran solution (2% w/v).

For all flowing fluids, the molecules are showing relative motion between one another, and this process is always combined with internal frictional forces. Therefore, for all fluids in motion, a certain flow resistance occurs which may be determined in terms of the viscosity. For ideally viscous fluids measured at a constant temperature, the value of the ratio of shear stress τ and corresponding shear rate γ, is a material constant and is designated as shear viscosity: $\eta = \tau/\gamma$.

Analysing the graph in Figure 20, it is possible to verify that the shear viscosity of kefiran solution decreases with the increment of shear rate, reaching the steady value of 0.4312 Pa.s (zero-shear viscosity). Two main areas were observed: (a) shear-thinning (pseudoplastic) behaviour, since the shear viscosity decreases with the shear rate and (b) a *Newtonian* region where the shear viscosity reaches a practically constant value for different shear rates. This *Newtonian* fluid behaviour at extreme shear rates is usual in many shear-thinning (pseudoplastic) fluids [6].

4.2. Kefiran and alginate particles

To obtain regular spherical shaped particles, crosslinking is a required phenomenon to occur. However, since kefiran alone cannot crosslink, it was necessary to add a compound that promotes crosslinking of the particles. Alginate is a natural ionic polysaccharide that can crosslink in the presence of divalent cations, for example calcium ions (Ca^{2+}). The specific and strong interaction between the calcium ions and the guluronic acid blocks of the alginate allows the gelation (formation of a three-dimensional

network). Calcium ions induce chain-chain association, being responsible for constituting junction zones responsible for alginate crosslinking [102]. In the techniques used to obtain kefiran/alginate particles, a 0.1 M calcium chloride solution was used. As such, the ionotropic gelation technique was tested. In this technique, the process of microdroplet hardening allows the production of particles due to the electrostatic interactions between two ionic species, where at least one of the species is a polymer [81, 82].

In the direct precipitation method, the kefiran and alginate solution was in a syringe and through human mechanical action, the solution was pushed until small drops were formed at the tip of the syringe. Then, these drops fell into the calcium chloride solution, crosslinked and formed particles.

To maximize the amount of kefiran present in the particles, different formulations with different percentages of kefiran (2% w/v) and alginate (1% w/v) were tested. Results are presented in Table 4.

Table 4. Formulations tested with different % (v/v) of kefiran (2% w/v) and alginate (1% w/v).

	Kefiran (%)	**Alginate (%)**	**Results**
Sol. A	90	10	Particles with irregular shape; poor viscoelastic properties
Sol. B	80	20	Particles with irregular shape; poor viscoelastic properties
Sol. C	66	33	Particles with irregular shape; poor viscoelastic properties
Sol. D	50	50	Microspheres with regular shape; good viscoelastic properties

The formulation with 90% kefiran and 10% alginate (Table 4, sol A) produced particles with irregular shape and poor viscoelastic properties. This also occurred with the following two formulations: 80% kefiran/20% alginate (sol B) and 66% kefiran/33% alginate (sol C). The formulation with equal percentage of kefiran and alginate (sol. D, Table 4) was the one that yielded best results, being obtained particles with regular shape

and good viscoelastic properties. The particles produced by this formulation are shown in Figure 21.

Figure 21. Particles composed of 50% kefiran (2% w/v) and 50 % alginate (1% w/v).

Afterwards, formulations with different percentages of the polymers were made, maintaining the solution of kefiran (2% w/v) but using an alginate solution more concentrated (2% w/v). Results are presented in Table 5.

Table 5. Formulations tested with different % (v/v) of kefiran (2% w/v) and alginate (2% w/v).

	Kefiran (%)	**Alginate (%)**	**Results**
Sol. A	90	10	Particles with irregular shape; poor viscoelastic properties
Sol. B	80	20	Microspheres with regular shape; good viscoelastic properties
Sol. C	70	30	Microspheres with regular shape; good viscoelastic properties
Sol. D	50	50	Microspheres with regular shape; good viscoelastic properties

Through the analysis of the data presented in Table 5, it is possible to infer that all the formulations resulted in particles with good shape and good viscoelastic properties, except the 90% kefiran/10% alginate (sol A) formulation. The maximization of kefiran in the particles was achieved with a formulation of 80% kefiran/20% alginate (sol B), both polymeric solutions at a 2% (w/v) concentration. Figure 22 shows the particles obtained.

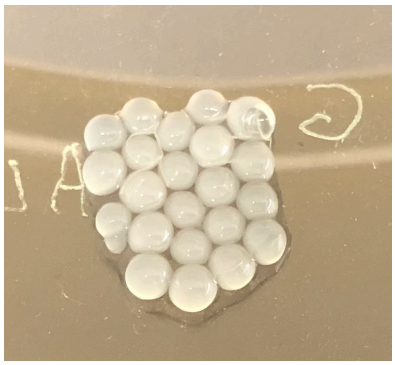

Figure 22. Particles composed of 50% kefiran (2% w/v) and 50% alginate (2% w/v).

However, since the particles produced by this method, had larger size than intended, a needle was fitted to the syringe to decrease it. Although this preparation method led to a significant reduction in the size of the particles, these were still visible to the naked eye. Therefore, other approaches to particle production were considered to overcome the particles size limitation of the manual extrusion technique, namely the use of a syringe pump. Three different concentrations of the kefiran and alginate solution were tested, namely: 2% (w/v), 1% (w/v) and 0.2% (w/v), where the percentage of each polymer in the solution varied (80% Kef/20% Alg and 50% Kef/50% Alg). The syringe contained the kefiran and alginate solution, being integrated in a pump. The force exerted on the syringe generated drops at the needle and these drops fell into a container with calcium chloride under magnetic stirring. Nevertheless, this technique did not generate particles, but small irregularly shaped fragments [Figure 23].

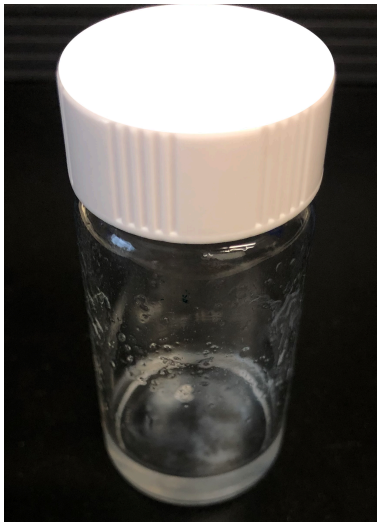

Figure 23. Fragments of particles produced by the ionotropic gelation technique.

Thus, another particle production technique, the microfluidic-based nanoprecipitation technique, was tested. The designed system had two microfluidic

pumps, being a syringe connected to each pump. The mechanical action exerted on the syringe is influenced by the flow rate of the solution, which was different in each pump [Figure 24].

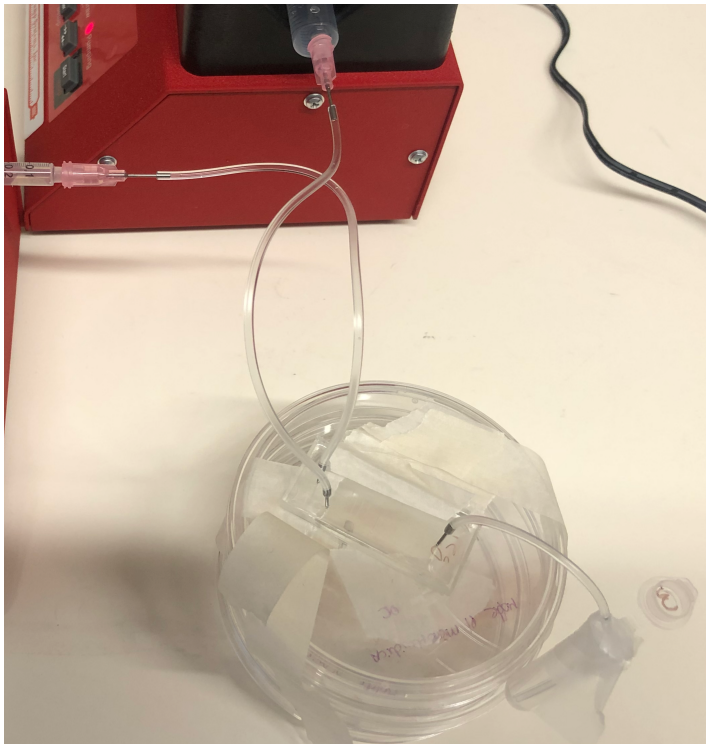

Figure 24. Microfluidic device setup.

A kefiran and alginate solution (50:50) with a concentration of 1% (w/v) was first tested, but no particles were obtained. This was most likely due to the high concentration of the solution, which caused the microfluidic chip to clog. Thus, the concentration of the solution was adjusted to 0.2% (w/v), in accordance with previous work performed by our group (Unpublished data).

The first strategy had the solution of kefiran and alginate in one of the syringes, calcium chloride solution on the other and, at the end of the system, Milli-Q® water, into which the particles fell. However, the crosslinking of particles within the microfluidic chip also occurred and blocked the flow, being this approach discarded. A new approach was designed, in which one of the syringes contained the kefiran and alginate solution, the other contained Milli-Q® water, and the calcium chloride solution was at the end of the system, where particles would crosslink and be collected. Contrary to the previous approach, the particles only cross-linked when in contact with the calcium chloride solution and, therefore, no clogging of the system occurred. Therefore, this method was

used for the production of kefiran/alginate nanoparticles (Kef/Alg NP) with and without the MSI-78 peptide (AMP).

The nanoparticles obtained were characterised by NTA and results are expressed on Table 6.

Table 6. NTA results for kefiran particles.

	Concentration (particles/mL)	Average size (nm)
Kef/Alg NP	1 x 10^{10}	106.6
Kef/Alg-AMP NP	1 x 10^{10}	85.2

The concentration of both batches is similar (1 x 10^{10} particles/mL) but the average particle size was different: Kef/Alg NP had an average size of 106.6 nm, while the size for those loaded with AMP (Kef/Alg-AMP NP) was smaller (85.2 nm) [103].

This difference may be related to the fact that kefiran and MSI-78 have opposite charges: kefiran as well as alginate are negatively charged while the MSI-78 peptide is positively charged [104]. Thus, electrostatic interaction can occur which may lead to the observed particle size reduction.

4.3. Kefiran and Alginate nanoparticles antibacterial performance

Two *H. pylori* strains (J99 and 26695) were tested against Kef/Alg NP and Kef/Alg-AMP NP (loaded with MSI-78). These two strains were selected since *H. pylori* J99 is a highly pathogenic strain, while *H. pylori* 26695 is less virulent and reported as more sensitive to the peptide MSI-78 [46].

The two *H. pylori* strains were exposed to Kef/Alg NP and Kef/Alg-AMP NP at 10^9, 10^8 and 10^7 particle/mL over 24 hours, 37 °C, 150 rpm. The results obtained for *H. pylori* J99 are shown in Figure 25.

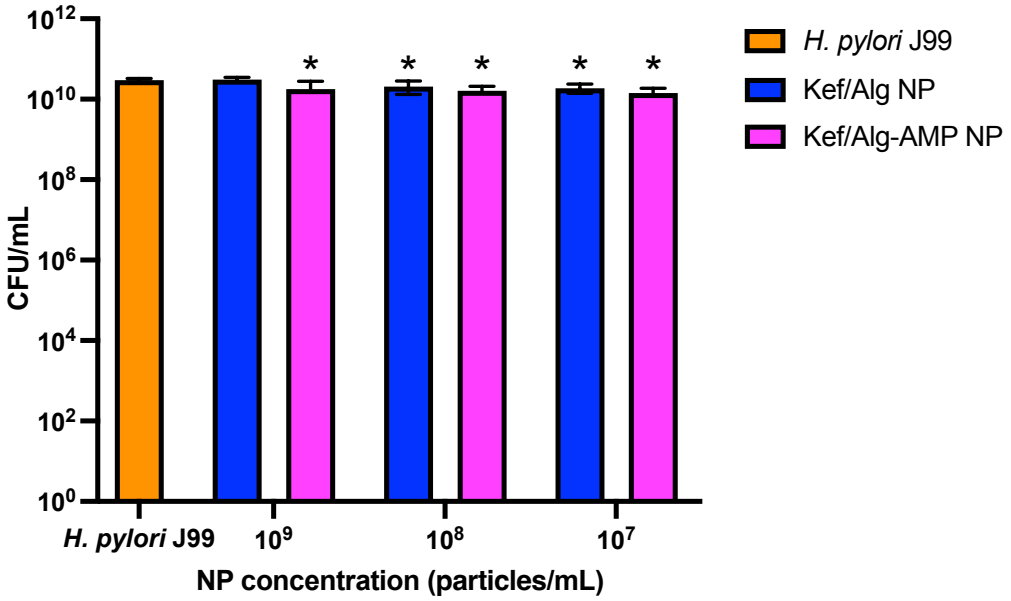

Figure 25. Activity of Kef/Alg NP and Kef/Alg-AMP NP against *H. pylori* J99 after 24 h (n=3), *: statistically significant different from the control ($p<0.05$).

A compound exhibits bacteriostatic behaviour when it prevents the growth of bacteria. On the other hand, bactericidal behaviour means that it is capable of killing the bacteria, being assumed that a 3-$\log_{10}$ reduction in CFUs/mL corresponds already to bactericidal effect [105]. As seen in figure 25, it is possible to conclude that Kef/Alg NP did not have bactericidal performance at the concentrations tested. However, Kef/Alg NP and Kef/Alg-AMP NP at 10^8 and 10^7 particle/mL reduced the bacterial load in comparison to the control culture with statistically significance ($p<0.05$). The fact that 10^9 particle/mL Kef/Alg NP did not significantly impacted *H. pylori* J99 and only lower concentrations (10^8 and 10^7 particle/mL) of the NP were able to reduce the bacterial load in comparison to the control may be related with the bacterial interaction with the nanoparticles: by having more nanoparticles, more aggregation may occur and particles might not be as available for bacterial interaction as when having a less concentrated solution. Moreover, Kef/Alg-AMP NP were able to significantly impact the bacterial load at all the concentrations tested, despite not reaching bactericidal performance.

The strain *H. pylori* 26695 was also tested and results are shown in Figure 26.

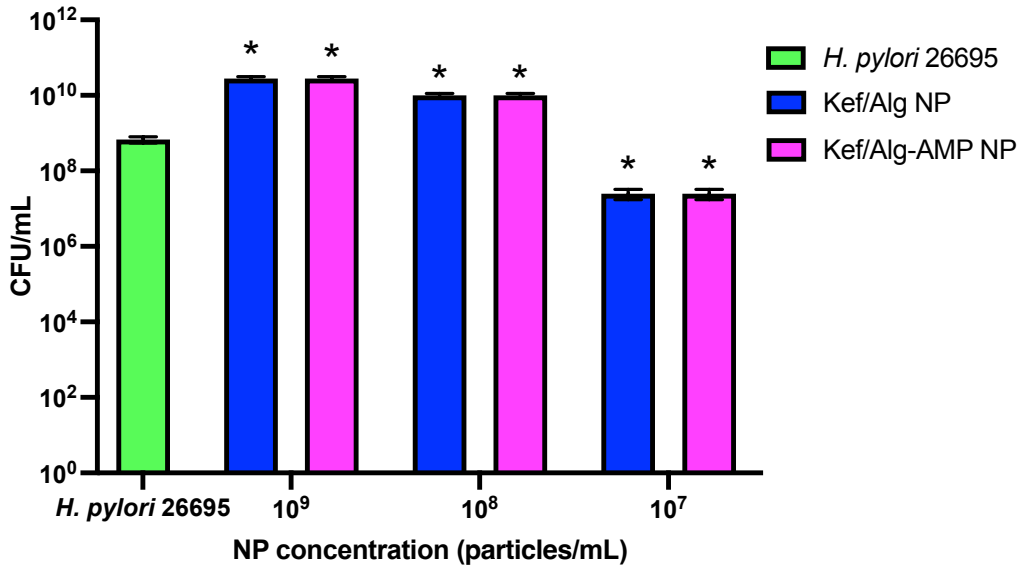

Figure 26. Activity of Kef/Alg NP and Kef/Alg-AMP NP against *H. pylori* 26695 after 24 h (n=3), *: statistically significant different from the control ($p<0.05$).

Kef/Alg NP and Kef/Alg-AMP NP at the concentration of 10^7 particles/mL reduced the bacterial load in comparison to the control culture (*H. pylori* 26695 pure culture) ($p<0.05$). Despite not reaching bactericidal effect (3 log reduction) this result is interesting and further highlights that using a NP less concentrated might promote more bacteria/nanoparticle interaction, yielding better performance than higher concentrations. However, it must be noted that after 24h under optimal growth conditions, the control culture was expected to reach a density of at least 10^{10} CFU/mL, as seen for *H. pylori* J99 [Figure 25] and in accordance with the duplication time of the bacteria. Therefore, the values obtained as statistically significant for 10^9 and 10^8 particles/mL, higher than the control, should take this fact in account, as most likely operator errors regarding the quantification of the control culture occurred (e.g: pipetting errors, manual count of colonies subjected to errors, etc…). Further assays should be performed to confirm these results.

The gut microbiota consists of organisms that live in the digestive tract of humans. The gut is engaged in dynamic interactions with a massive microbial community in conditions that should permit homeostasis [106]. A variety of bacteria are part of it, including *E. coli* and *L. acidophilus* [89]. One of the main drawbacks associated with the common antibiotherapy targeting *H. pylori* is the destruction of the normal gut microbiota. As such, the designed Kef/Alg NP and Kef/Alg-AMP NP were tested with these two bacteria representatives of the microbiome to understand its safety/interaction.

For that, the same concentration (10^9, 10^8 and 10^7 particles/mL) assayed against *H. pylori* were evaluated. Moreover, the nanoparticles were incubated with bacteria representative of the gut microbiota in either PBS or culture media. PBS does not possess the necessary nutrients for normal bacterial growth, it simply provides a stable environment to keep bacterial cells viable until transferred to more suitable conditions [107]. As such, assays were carried out in PBS to verify the effect of NP in an environment where bacteria cannot thrive and where the occurrence of a protein corona that might delay the NP performance is unlikely [107].

Results obtained for *E. coli* are shown in Figure 27 (PBS) and Figure 28 (culture medium).

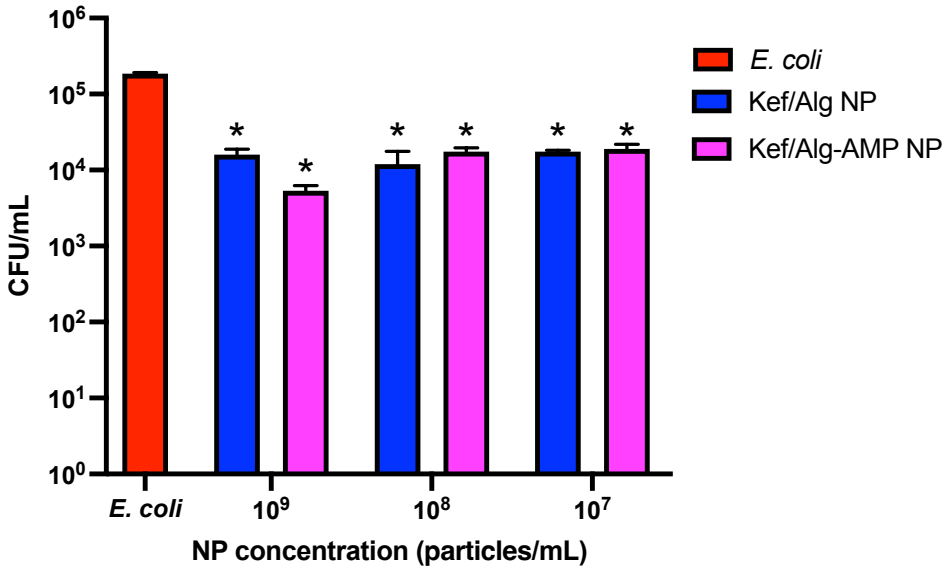

Figure 27. Activity of Kef/Alg NP and Kef/Alg-AMP NP against *E. coli* after 2 h in PBS (n=3), *: statistically significant different from the control ($p<0.05$).

A statistically significant reduction in the value of CFUs/mL for all the NP concentrations tested when compared to the control culture (*E. coli*) was seen for both NP (Kef/Alg NP and Kef/Alg-AMP NP) [Figure 27]. It can be hypothesized that, if the nanoparticles were allowed to interact longer, a bactericidal effect (reduction of 3 log) would be observed.

Regarding the assay of *E. coli* in culture medium, the results obtained are depicted in Figure 28.

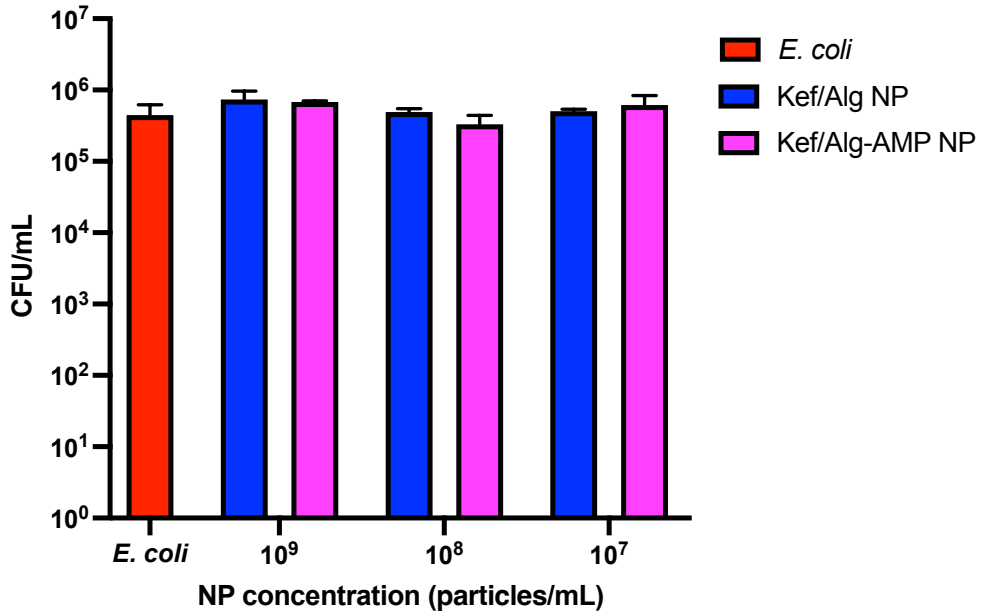

Figure 28. Activity of Kef/Alg NP and Kef/Alg-AMP NP against *E. coli* after 2 h in culture medium (n=3).

Contrary to what was seen in PBS [Figure 27], none of the nanoparticles showed any tendency to have antibacterial performance against *E. coli*, as the CFU/mL values are similar to the control (*E. coli*). This result highlights that in culture media the NP action may be hindered by the corona proteins. This corona consists of a biomolecular shell that forms on the surface of NP during their interactions with biological fluids. In fact, a huge limitation of the NP is their fate *in vivo* due to formation of "protein corona" as the molecular properties and composition of the protein corona affect the cellular uptake of NP [107].

Lactobacillus acidophilus was also tested, as a Gram-positive bacteria representative of the gut microbiome. The results are shown in Figure 29.

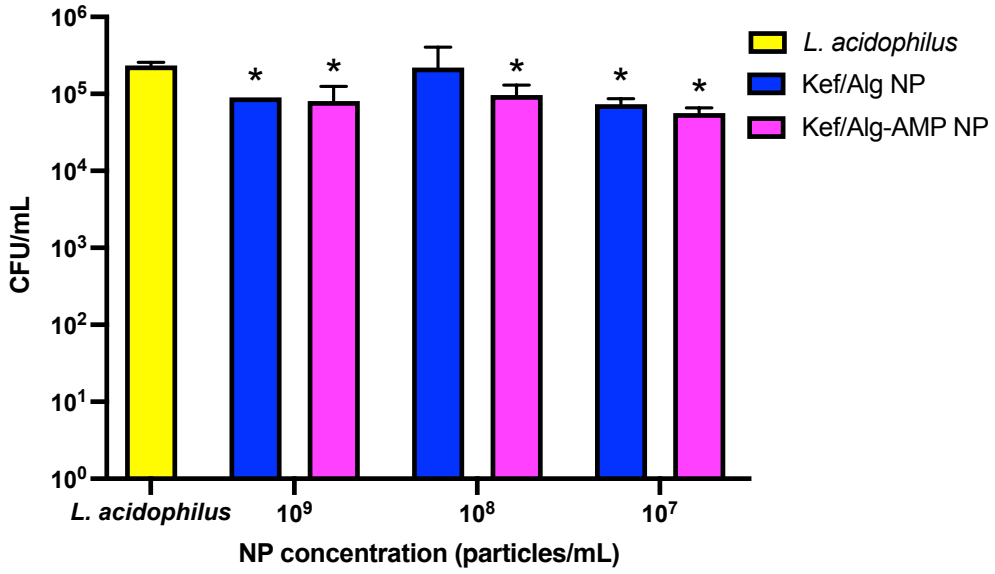

Figure 29. Activity of Kef/Alg NP and Kef/Alg-AMP NP against *L. acidophilus* after 2 h in PBS (n=3), *: statistically significant different from the control ($p<0.05$).

A slight reduction in the value of CFUs/mL for NP concentrations when compared with the control (*L. acidophilus*) is observable. All results obtained, except for the 10^8 particles/mL concentration for the Kef/Alg NP, were statistically significant ($p<0.05$).

The data obtained from the antibacterial performance assay in culture media is shown in Figure 30.

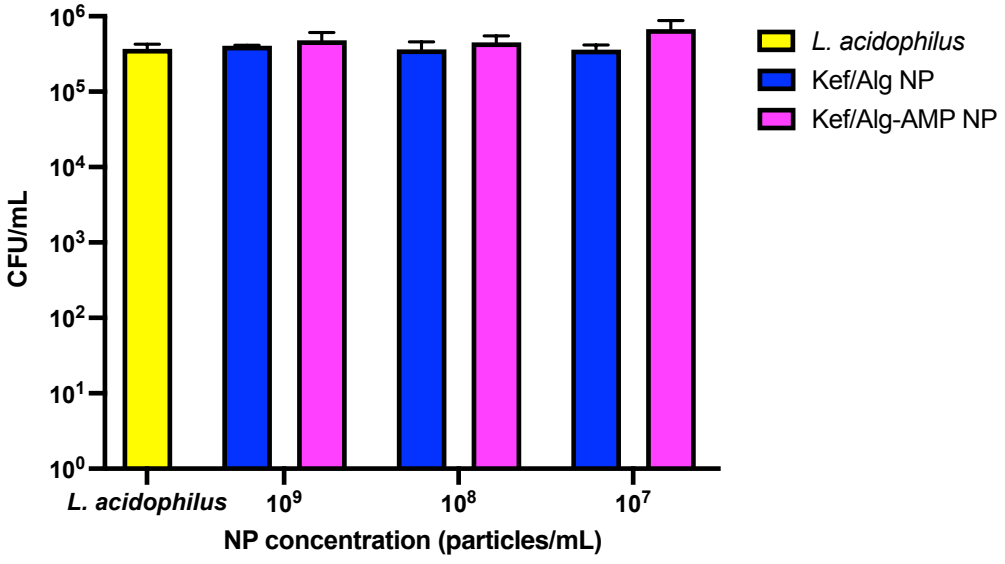

Figure 30. Activity of Kef/Alg NP and Kef/Alg-AMP NP against *L. acidophilus* after 2 h in culture medium (n=3).

None of the designed nanoparticles in the concentration range tested had effect, as the CFU/mL values at different concentrations were in the order of magnitude of the

control or even higher. Once again, the importance of the protein corona in masking the NP is highlighted.

Overall, in the experimental conditions used, none of the particles was bactericidal against either strain of *H. pylori*, *L. acidophilus* and *E. coli*, since a 3-$\log_{10}$ reduction in CFUs/mL was not observed. Also, at the concentrations and experimental settings used, the results obtained for *L. acidophilus* and *E. coli* are not encouraging in what concerns the safety of this approach to other gut bacteria, as their growth/viability was impacted. Further assays should be performed to certify this and fine tuning of the particles could be envisioned to overcome this interaction.

4.4. Peptide release

The fact that no antibacterial effect was observed for the nanoparticles loaded with MSI-78 (Kef/Alg-AMP NP) came across as surprising, since it is reported in the literature its effect against *H. pylori*. As such, the peptide release from the NP was studied. To release the peptide from the particles, it was necessary to break the crosslinking between alginate and the calcium chloride, being used EDTA at a concentration of 50 mM for that purpose [108]. The peptide release was evaluated after 2h, 24h and 48h. The concentration of the peptide present in the supernatant of each of the samples was determined by reading the absorbance (205 nm) of the supernatant of each of the samples and plotting against a calibration curve as described [84]. Then, the difference between the initial concentration (2 mg/mL) of peptide introduced in the kefiran and alginate solution and the concentration of peptide present in the supernatant allowed to determine the percentage of peptide released [Table 7]. As a control, NP immersed only in PBS were used.

Table 7. Peptide release quantification assays.

Sample	Time (h)	Abs (λ= 600 nm)	Peptide in the supernatant (µg/mL)	Release (%)
PBS	2	0.35	50	2.3
PBS + EDTA	2	19.8	780	39.2
PBS	24	0.28	40	2.1

PBS + EDTA	24	14.1	570	28.4
PBS	48	0.49	50	2.5
PBS + EDTA	48	20.7	820	40.8

In all assays, the samples with EDTA presented higher values for peptide release compared to those without EDTA, as expected. After 24h, the value obtained for the peptide release is lower than the one obtained after 2h assays. This was not expected and may be associated with operator errors.

After 48h, all the encapsulated peptide is expected to be released. In fact, the highest percentage of peptide release was obtained after 48h. Also, the obtained results suggest that the encapsulation yield of the peptide was 40% (maximum amount released). As such, it was possible to demonstrate that the peptide was successfully encapsulated on the designed NP.

These results also account for the lack of antimicrobial activity reported against *H. pylori*. The MIC (Minimum Inhibitory Concentration) corresponds to the minimum concentration at which an antibiotic agent, under strictly controlled *in vitro* conditions, completely prevents the visible growth of an organism [109]. The MIC value of MSI-78 for *H. pylori* J99 is 256 μg/mL and 64 μg/mL for *H. pylori* 26695 strain [86]. Comparing the values of the concentration of the peptide present in the supernatant with the MIC of the MSI-78 for each of the strains, the values obtained in EDTA after 2h (780 μg/mL), EDTA after 24h (570 μg/mL) and EDTA after 48h (820 μg/mL) assays are both greater than the MIC. However, when not using EDTA, i.e, not promoting the rupture of the NP crosslinking, the maximum value obtained was 50 μg/mL [Table 7], lower than the MIC for both strains. Nonetheless, as demonstrated by the EDTA assays, the amount of peptide encapsulated was enough to reach antibacterial effect. To overcome this drawback, one of the options would be to decrease the concentration of the calcium chloride solution, which would lead to less crosslinking of the particles. Furthermore, other compounds capable of breaking crosslinking, allowing the release of the encapsulated peptide, would be interesting to explore, since EDTA has a cytotoxic effect [110].

4.5. Resazurin Assay

The resazurin assay, also called Alamar Blue®, allows a rapid, simple and sensitive measurement of the viability of bacteria and mammalian cells. Since living cells are metabolically active, these are able to reduce the nonfluorescent dye resazurin to the strongly-fluorescent dye resorufin, through mitochondrial reductase. The fluorescence emitted is proportional to the number of viable cells [111].

A resazurin assay was performed to evaluate the cytocompatibility of a kefiran solution on AGS cells. Various concentrations of kefiran were tested namely, 10, 5, 2.5 and 1.25 mg/mL. Each of these concentrations had 2 wells assigned. In addition, positive and negative cell controls, kefiran solution and cell culture medium controls were established. The large white square surrounds the wells with cells for the four kefiran concentrations and the white rectangle encompasses the positive cell controls [Figure 31].

Figure 31. Resazurin assay plate.

The cell viability results calculated using (eq. 1) are represented on Figure 32.

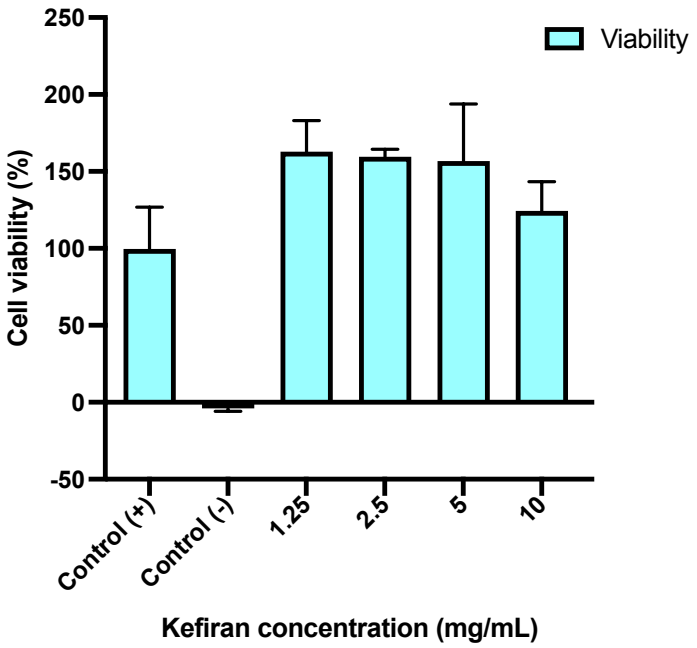

Figure 32. Cell viability after exposure to kefiran solutions with different concentrations.

As seen in Figure 32, kefiran did not present cytotoxicity towards AGS cells (no statistically significant differences were observed towards the positive control, AGS cells; $p<0.05$).

These results confirm kefiran safety in accordance to what was previously shown in the literature [6].

4.6. Kefiran discs

Other approaches to kefiran were explored by the development of discs. These discs were obtained through lyophilization of the kefiran solution present in the wells. The kefiran discs produced are shown in Figure 33.

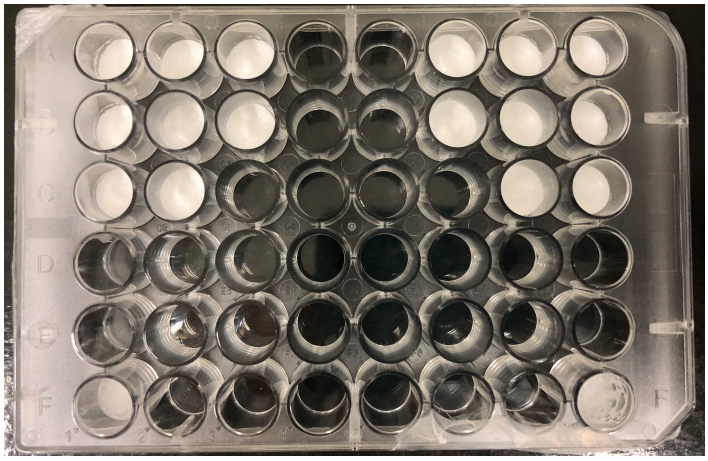

Figure 33. Plate with kefiran discs.

In order to analyse the characteristics and structure of the discs produced, a SEM analysis was performed. The results obtained are shown in Figure 34.

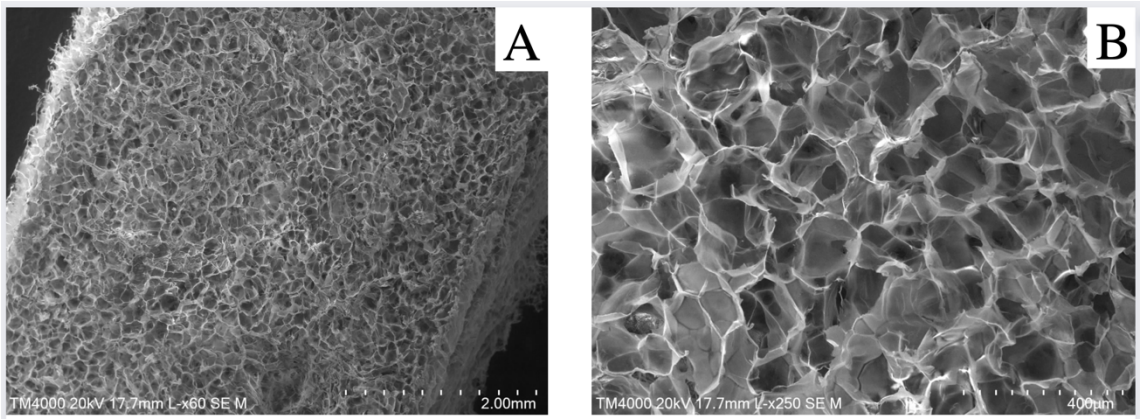

Figure 34. SEM analysis: (A) 60x magnification, (B) 250x magnification.

Scaffolds, typically made of polymeric biomaterials, are porous 3D structures with interconnectivity of the porous, that function as a template for tissue formation, normally, a mimicry of the extracellular matrix for cells to attach and subsequent tissue development. These structures provide both physical and biochemical cues for cells to adhere, proliferate and differentiate into the needed cell types [112].

The developed discs have characteristics that would suit them as scaffolds. For instance, the discs have a porous structure with interconnectivity between the pores [Figure 34] that will allow cell nutrition, migration and proliferation, as well as vascularization, essential features for tissue regeneration to occur.

Furthermore, kefiran is biodegradable, making the application of these discs feasible, as the scaffold should gradually degrade. However, the actual behaviour of the discs would only be evaluated when implementing them in a tissue regeneration situation.

One of the main issues of biomaterials design for tissue engineering applications is their mechanical properties, namely its viscoelasticity, and rheological tests give important information on that. Rheological experiments do not merely reveal information about flow behaviour of liquids but also about deformation behaviour of solids, since a large deformation produced by shear forces causes many materials to flow. The behaviour of all real materials is based on the combination of both a viscous and an elastic portion and, therefore, it is called viscoelastic. Frequency sweeps are oscillatory tests performed at variable frequencies, keeping the amplitude at a constant value (and also the measuring temperature) and are used to investigate time-dependent deformation behaviour since the

frequency is the inverse value of time [113]. In a shear stress cycle, it is possible to determine the storage modulus (*G*') which is related to the deformation energy stored, i.e. the material stiffness and the loss modulus (*G*''), which is related to the deformation energy dissipated, i.e. the flow or liquid-like response. The storage modulus depends on the rigidity of the macromolecules and their entanglement, while the loss modulus depends on the bonds, which control conformational changes in chain segments and the displacement of one chain in relation to another [114]. The damping factor or loss factor (tan δ) is measured by determining the ratio G'/G''. Frequency sweep curves obtained from oscillatory shear measurements performed on the kefiran scaffolds are shown in Figure 35, revealing the dependence of G' and G" upon the frequency. It is observed that the kefiran scaffolds response practically do not depend on the strain. Both *G*' and *G*'' exhibit a constant plateau between 0.01 Hz and 1 Hz while slightly decreasing as the frequency increased from 1 Hz to 10 Hz, being the behaviour well within the linear viscoelastic region. It is also observed that the storage modulus is higher than the loss modulus and consequently, tan δ >1, indicating that kefiran scaffolds behaves like an elastic solid, an extremely important feature for tissue engineering applications [Figure 35].

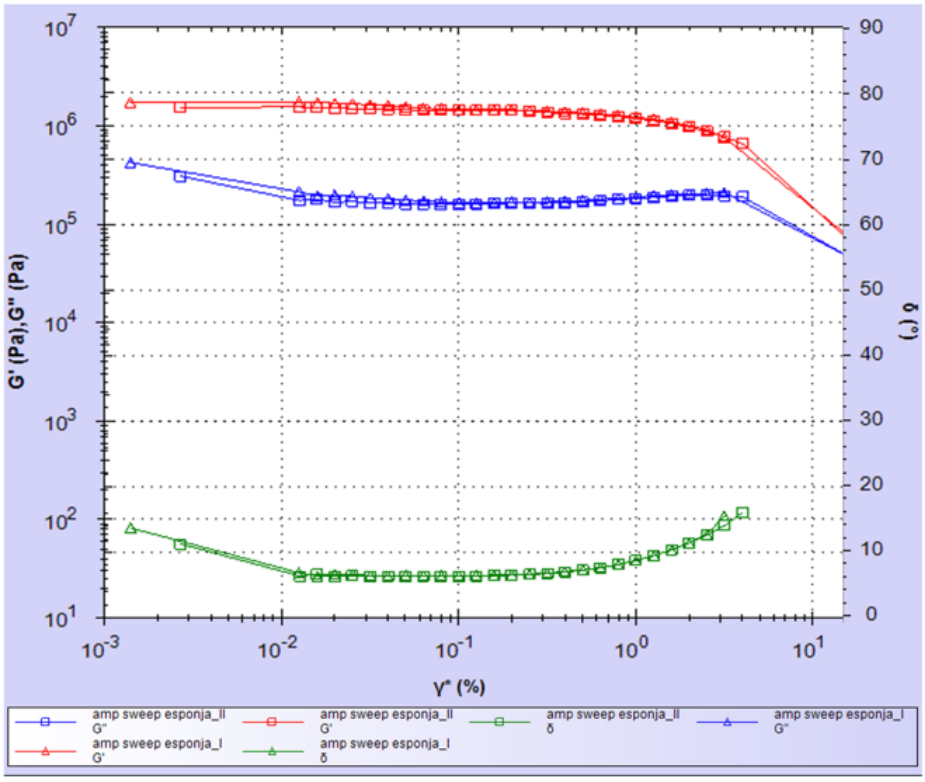

Figure 35. Elastic modulus, viscous modulus and tan delta versus shear strain for kefiran scaffolds.

CHAPTER 5 – CONCLUDING REMARKS

5. Concluding remarks

5.1. Conclusions

In this work it was possible to optimize the kefiran production method, namely the temperatures used for its extraction. This preparation method of kefiran allowed to obtain a pure polymer as evidenced by FTIR, CRM, DSC and TGA analysis.

Different kefiran/alginate ratios were tested to obtain particles, being 80% the maximum kefiran percentage allowed. Nanoparticles of kefiran and alginate were successfully prepared using microfluidics. Additionally, peptide incorporation into the nanoparticles was accomplished.

The activity of the nanoparticles produced was evaluated against the gastric pathogen *Helicobacter pylori* and bacteria representative of a normal gut microbiome, *Escherichia coli* and *Lactobacillus acidophilus*. *H. pylori* strains tested were not significantly impacted by the NP, either with or without the antimicrobial peptide. This fact was later demonstrated to be linked to the low release of the peptide from the Kef/Alg AMP-NP. However, *E. coli* and *L. acidophilus* showed that when exposed to the designed particles without action of a protein corona (assays in PBS), these NP would interfere with their growth/viability. Nonetheless, after fine-tuning to overcome the Kef/Alg-NP and Kef/Alg AMP-NP interaction with bacteria from the gut microbiota, such as adding a target moiety to *H. pylori* on the NP surface, these can still be considered to release peptides or other compounds with antimicrobial properties. In addition, kefiran solutions were shown to be cytocompatible.

Concerning the kefiran discs, porous scaffolds with interconnected porosity were obtained after kefiran lyophilization, suggesting its biomedical potential in tissue engineering applications. Additionally, kefiran scaffolds behaves like an elastic solid, an extremely important characteristic for tissue engineering applications.

As a general conclusion, this work allowed to establish a protocol for kefiran nanoparticles production and to further explore this exopolysaccharide, namely its antibacterial effect and different approaches to its use.

5.2. Future work

Since the time to develop this work was limited, in the future, the preparation of nanoparticles with the maximum effective percentage of kefiran would be relevant. Also, alginates with different degradation rates, i.e. different molecular weights, should be tested to access changes in the behaviour of nanoparticles. It would also be interesting to carry out a different formulation of the particles namely, to explore the combination of kefiran with different polymers alternatively to alginate. A Transmission Electron Microscopy (TEM) analysis would allow to understand the interaction between the nanoparticles and bacteria. Since the stomach has an acidic pH, it would be interesting to evaluate the behaviour of nanoparticles in a low pH, which might lead to burst and consequent release of the peptide.

Moreover, it would also be important to study the designed nanoparticles cytocompatibility. In addition, the antibacterial properties of kefiran discs would also be interesting to explore.

Furthermore, analysis like Nuclear Magnetic Resonance would allow to understand more deeply the interaction between alginate and kefiran (on-going studies).

5.3. Comments

Unlike the curricular project of the BSc, this thesis allowed me to develop a practical work that was highly beneficial as it allowed me also to deal with all materials and devices directly. As such, it was possible to experience the daily life of a researcher, with all the adversities and benefits that it involves.

The fact that the project is incorporated into the Biomedical Engineering master has several benefits as it promotes the expansion of scientific knowledge and the development of new skills that will be of real importance for future works and projects. After the development of the project and a general evaluation of all the work done, it is possible to state that the overall balance is positive. Furthermore, it has a contribution role for the Scientific Community, namely in the exploration of new compounds/strategies to fight bacteria.

Bibliography and sources of information

[1] D. Joe Dailin *et al.*, "Biosynthesis, Production and Application Of Kefiran In Food Industry: A Review," *Bioscience Research,* vol. 18, pp. 102-119, 08/25 2021.

[2] S. Plessas, C. Nouska, I. Mantzourani, Y. Kourkoutas, A. Alexopoulos, and E. Bezirtzoglou, "Microbiological Exploration of Different Types of Kefir Grains," *Fermentation,* vol. 3, no. 1, p. 1, 2017. [Online]. Available: https://www.mdpi.com/2311-5637/3/1/1.

[3] N. F. Azizi *et al.*, "Kefir and Its Biological Activities," (in eng), *Foods,* vol. 10, no. 6, May 27 2021, doi: 10.3390/foods10061210.

[4] S. Arslan, "A review: chemical, microbiological and nutritional characteristics of kefir," *CyTA - Journal of Food,* vol. 13, no. 3, pp. 340-345, 2015/07/03 2015, doi: 10.1080/19476337.2014.981588.

[5] G. Sathiyanarayanan, K. Dineshkumar, and Y. H. Yang, "Microbial exopolysaccharide-mediated synthesis and stabilization of metal nanoparticles," (in eng), *Crit Rev Microbiol,* vol. 43, no. 6, pp. 731-752, Nov 2017, doi: 10.1080/1040841x.2017.1306689.

[6] H. Radhouani, C. Gonçalves, F. Maia, J. Oliveira, and R. L. Reis, "Kefiran biopolymer: Evaluation of its physicochemical and biological properties," *Journal of Bioactive and Compatible Polymers,* vol. 33, p. 088391151879391, 08/18 2018, doi: 10.1177/0883911518793914.

[7] Z. Moradi and N. Kalanpour, "Kefiran, a branched polysaccharide: Preparation, properties and applications: A review," *Carbohydrate Polymers,* vol. 223, p. 115100, 2019/11/01/ 2019, doi: https://doi.org/10.1016/j.carbpol.2019.115100.

[8] S. S. Esnaashari, S. Rezaei, E. Mirzaei, H. Afshari, S. M. Rezayat, and R. Faridi-Majidi, "Preparation and characterization of kefiran electrospun nanofibers," (in eng), *Int J Biol Macromol,* vol. 70, pp. 50-6, Sep 2014, doi: 10.1016/j.ijbiomac.2014.06.014.

[9] I. Shahabi-Ghahfarrokhi, F. Khodaiyan, M. Mousavi, and H. Yousefi, "Effect of γ-irradiation on the physical and mechanical properties of kefiran biopolymer film," *International Journal of Biological Macromolecules,* vol. 74, pp. 343-350, 2015/03/01/ 2015, doi: https://doi.org/10.1016/j.ijbiomac.2014.11.038.

[10] M. Mohd Nadzir, R. W. Nurhayati, F. N. Idris, and M. H. Nguyen, "Biomedical Applications of Bacterial Exopolysaccharides: A Review," (in eng), *Polymers (Basel),* vol. 13, no. 4, Feb 10 2021, doi: 10.3390/polym13040530.

[11] K.-X. Tan, V. N. Chamundeswari, and S. C. J. Loo, "Prospects of kefiran as a food-derived biopolymer for agri-food and biomedical applications," *RSC Advances,* 10.1039/D0RA02810J vol. 10, no. 42, pp. 25339-25351, 2020, doi: 10.1039/D0RA02810J.

[12] M. A. Sabatino *et al.*, "Development of injectable and durable kefiran hydro-alcoholic gels," *International Journal of Biological Macromolecules,* vol. 149, pp. 309-319, 2020/04/15/ 2020, doi: https://doi.org/10.1016/j.ijbiomac.2020.01.244.

[13] L. Marangoni Júnior, R. P. Vieira, and C. A. R. Anjos, "Kefiran-based films: Fundamental concepts, formulation strategies and properties," (in eng), *Carbohydr Polym,* vol. 246, p. 116609, Oct 15 2020, doi: 10.1016/j.carbpol.2020.116609.

[14] H. Radhouani, C. Gonçalves, F. R. Maia, J. M. Oliveira, and R. L. Reis, "Biological performance of a promising Kefiran-biopolymer with potential in regenerative medicine applications: a comparative study with hyaluronic acid," (in eng), *J Mater Sci Mater Med,* vol. 29, no. 8, p. 124, Jul 26 2018, doi: 10.1007/s10856-018-6132-7.

[15] L. M. Blandón, G. A. Islan, G. R. Castro, M. D. Noseda, V. Thomaz-Soccol, and C. R. Soccol, "Kefiran-alginate gel microspheres for oral delivery of ciprofloxacin," (in eng), *Colloids Surf B Biointerfaces,* vol. 145, pp. 706-715, Sep 1 2016, doi: 10.1016/j.colsurfb.2016.05.078.

[16] J. Piermaria, G. Diosma, C. Aquino, G. Garrote, and A. Abraham, "Edible kefiran films as vehicle for probiotic microorganisms," *Innovative Food Science & Emerging Technologies,* vol. 32, pp. 193-199, 2015/12/01/ 2015, doi: https://doi.org/10.1016/j.ifset.2015.09.009.

[17] M. Murofushi, M. Shiomi, and K. Aibara, "Effect of orally administered polysaccharide from kefir grain on delayed-type hypersensitivity and tumor growth in mice," (in eng), *Jpn J Med Sci Biol,* vol. 36, no. 1, pp. 49-53, Feb 1983, doi: 10.7883/yoken1952.36.49.

[18] K. L. Rodrigues, J. C. T. Carvalho, and J. M. Schneedorf, "Anti-inflammatory properties of kefir and its polysaccharide extract," *InflammoPharmacology,* vol. 13, no. 5, pp. 485-492, 2005/10/01 2005, doi: 10.1163/156856005774649395.

[19] H. Maeda, H. Mizumoto, M. Suzuki, and K. Tsuji, "Effects of Kefiran-Feeding on Fecal Cholesterol Excretion, Hepatic Injury and Intestinal Histamine Concentration in Rats," *Bioscience and Microflora,* vol. 24, no. 2, pp. 35-40, 2005, doi: 10.12938/bifidus.24.35.

[20] H. Radhouani, D. Bicho, C. Gonçalves, F. Maia, R. L. Reis, and J. Oliveira, "Kefiran cryogels as potential scaffolds for drug delivery and tissue engineering applications," *Materials Today Communications,* vol. 20, p. 100554, 06/01 2019, doi: 10.1016/j.mtcomm.2019.100554.

[21] M. Zolfi, F. Khodaiyan, M. Mousavi, and M. Hashemi, "The improvement of characteristics of biodegradable films made from kefiran-whey protein by nanoparticle incorporation," (in eng), *Carbohydr Polym,* vol. 109, pp. 118-25, Aug 30 2014, doi: 10.1016/j.carbpol.2014.03.018.

[22] Z. Vinarov *et al.*, "Impact of gastrointestinal tract variability on oral drug absorption and pharmacokinetics: An UNGAP review," (in eng), *Eur J Pharm Sci,* vol. 162, p. 105812, Jul 1 2021, doi: 10.1016/j.ejps.2021.105812.

[23] Y. Xu, N. Shrestha, V. Préat, and A. Beloqui, "Overcoming the intestinal barrier: A look into targeting approaches for improved oral drug delivery systems," (in eng), *J Control Release,* vol. 322, pp. 486-508, Jun 10 2020, doi: 10.1016/j.jconrel.2020.04.006.

[24] S. Hua, "Advances in Oral Drug Delivery for Regional Targeting in the Gastrointestinal Tract - Influence of Physiological, Pathophysiological and Pharmaceutical Factors," (in English), *Frontiers in Pharmacology,* Review vol. 11, 2020-April-28 2020, doi: 10.3389/fphar.2020.00524.

[25] F. Serafini *et al.*, "Kefir fermented milk and kefiran promote growth of Bifidobacterium bifidum PRL2010 and modulate its gene expression," (in eng), *Int J Food Microbiol,* vol. 178, pp. 50-9, May 16 2014, doi: 10.1016/j.ijfoodmicro.2014.02.024.

[26] S. Khan *et al.*, "Fourier Transform Infrared Spectroscopy: Fundamentals and Application in Functional Groups and Nanomaterials Characterization," 2019.

[27] S. Gomes da Costa, A. Richter, U. Schmidt, S. Breuninger, and O. Hollricher, "Confocal Raman microscopy in life sciences," (in eng), *Morphologie,* vol. 103, no. 341, pp. 11-16, Mar 2019, doi: 10.1016/j.morpho.2018.12.003.

[28] S. Tott *et al.*, "Raman imaging-based phenotyping of murine primary endothelial cells to identify disease-associated biochemical alterations," *Biochimica et Biophysica Acta (BBA) - Molecular Basis of Disease,* vol. 1867, no. 9, p. 166180, 2021/09/01/ 2021, doi: https://doi.org/10.1016/j.bbadis.2021.166180.

[29] J. Abraham, A. P. Mohammed, M. P. Ajith Kumar, S. C. George, and S. Thomas, "Chapter 8 - Thermoanalytical Techniques of Nanomaterials," in *Characterization of Nanomaterials*, S. Mohan Bhagyaraj, O. S. Oluwafemi, N. Kalarikkal, and S. Thomas Eds.: Woodhead Publishing, 2018, pp. 213-236.

[30] N. Sizochenko, A. Mikolajczyk, M. Syzochenko, T. Puzyn, and J. Leszczynski, "Zeta potentials (ζ) of metal oxide nanoparticles: A meta-analysis of experimental data and a predictive neural networks modeling," (in eng), *NanoImpact,* vol. 22, p. 100317, Apr 2021, doi: 10.1016/j.impact.2021.100317.

[31] S. Samimi, N. Maghsoudnia, R. B. Eftekhari, and F. Dorkoosh, "Chapter 3 - Lipid-Based Nanoparticles for Drug Delivery Systems," in *Characterization and Biology of Nanomaterials for Drug Delivery*, S. S. Mohapatra, S. Ranjan, N. Dasgupta, R. K. Mishra, and S. Thomas Eds.: Elsevier, 2019, pp. 47-76.

[32] J. Abraham, T. Sharika, R. K. Mishra, and S. Thomas, "14 - Rheological characteristics of nanomaterials and nanocomposites," in *Micro and Nano Fibrillar Composites (MFCs and NFCs) from Polymer Blends*, R. K. Mishra, S. Thomas, and N. Kalarikkal Eds.: Woodhead Publishing, 2017, pp. 327-350.

[33] A. Taguet, "Chapter 16 - Rheological characterization of compatibilized polymer blends," in *Compatibilization of Polymer Blends*, A. A.R and S. Thomas Eds.: Elsevier, 2020, pp. 453-487.

[34] D. Griffiths, P. Carnell-Morris, and M. Wright, "Nanoparticle Tracking Analysis for Multiparameter Characterization and Counting of Nanoparticle Suspensions," (in eng), *Methods Mol Biol,* vol. 2118, pp. 289-303, 2020, doi: 10.1007/978-1-0716-0319-2_22.

[35] M. E. M. Parsons *et al.*, "A Protocol for Improved Precision and Increased Confidence in Nanoparticle Tracking Analysis Concentration Measurements between 50 and 120 nm in Biological Fluids," (in English), *Frontiers in Cardiovascular Medicine,* Original Research vol. 4, 2017-November-03 2017, doi: 10.3389/fcvm.2017.00068.

[36] K. Parvez, "Chapter 2 - Characterization Techniques of Two-Dimensional Nanomaterials," in *Biomedical Applications of Graphene and 2D Nanomaterials*, M. Nurunnabi and J. R. McCarthy Eds.: Elsevier, 2019, pp. 27-41.

[37] D. Lopes, C. Nunes, M. C. Martins, B. Sarmento, and S. Reis, "Eradication of Helicobacter pylori: Past, present and future," (in eng), *J Control Release,* vol. 189, pp. 169-86, Sep 10 2014, doi: 10.1016/j.jconrel.2014.06.020.

[38] , in *Helicobacter pylori: Physiology and Genetics*, H. L. T. Mobley, G. L. Mendz, and S. L. Hazell Eds. Washington (DC): ASM Press

Copyright © 2001, ASM Press., 2001.

[39] G. B. Cole, T. J. Bateman, and T. F. Moraes, "The surface lipoproteins of gram-negative bacteria: Protectors and foragers in harsh environments," (in eng), *J Biol Chem,* vol. 296, p. 100147, Jan-Jun 2021, doi: 10.1074/jbc.REV120.008745.

[40] Y. K. Wang *et al.*, "Diagnosis of Helicobacter pylori infection: Current options and developments," (in eng), *World J Gastroenterol,* vol. 21, no. 40, pp. 11221-35, Oct 28 2015, doi: 10.3748/wjg.v21.i40.11221.

[41] F. Ernst, "Transcriptional Regulation of the Nickel and Iron Metabolism in Helicobacter pylori," 01/01 2005.

[42] H. Enroth, W. Kraaz, L. Engstrand, O. Nyrén, and T. Rohan, "Helicobacter pylori Strain Types and Risk of Gastric Cancer: A Case-Control Study1," *Cancer Epidemiology, Biomarkers & Prevention,* vol. 9, no. 9, pp. 981-985, 2000.

[43] S. Censini *et al.*, "cag, a pathogenicity island of Helicobacter pylori, encodes type I-specific and disease-associated virulence factors," (in eng), *Proc Natl Acad Sci U S A,* vol. 93, no. 25, pp. 14648-53, Dec 10 1996, doi: 10.1073/pnas.93.25.14648.

[44] A. Covacci, S. Falkow, D. E. Berg, and R. Rappuoli, "Did the inheritance of a pathogenicity island modify the virulence of Helicobacter pylori?," (in eng), *Trends Microbiol,* vol. 5, no. 5, pp. 205-8, May 1997, doi: 10.1016/s0966-842x(97)01035-4.

[45] S. S. Duncan *et al.*, "Comparative genomic analysis of East Asian and non-Asian Helicobacter pylori strains identifies rapidly evolving genes," (in eng), *PLoS One,* vol. 8, no. 1, p. e55120, 2013, doi: 10.1371/journal.pone.0055120.

[46] P. S. Sampaio and C. R. C. Calado, "Potential of FTIR-Spectroscopy for Drugs Screening against Helicobacter pylori," (in eng), *Antibiotics (Basel),* vol. 9, no. 12, Dec 12 2020, doi: 10.3390/antibiotics9120897.

[47] Y. Sun and J. Zhang, "Helicobacter pylori recrudescence and its influencing factors," *Journal of Cellular and Molecular Medicine,* vol. 23, 09/01 2019, doi: 10.1111/jcmm.14682.

[48] I. Duś-Ilnicka, T. Dobosz, A. Manzin, G. Loi, C. Serra, and M. Radwan-Oczko, "Role of PCR in Helicobacter pylori diagnostics and research - New approaches for study of coccoid and spiral forms of the bacteria," *Postępy higieny i medycyny doświadczalnej (Online),* vol. 67, pp. 261-8, 01/11 2013, doi: 10.5604/17322693.1044005.

[49] Y. Matsuo, Y. Kido, and Y. Yamaoka, "Helicobacter pylori Outer Membrane Protein-Related Pathogenesis," (in eng), *Toxins (Basel),* vol. 9, no. 3, Mar 11 2017, doi: 10.3390/toxins9030101.

[50] S. Khan *et al.*, "Potential utility of nano-based treatment approaches to address the risk of Helicobacter pylori," *Expert Review of Anti-infective Therapy,* vol. 20, pp. 1-18, 10/18 2021, doi: 10.1080/14787210.2022.1990041.

[51] J. G. Kusters, A. H. van Vliet, and E. J. Kuipers, "Pathogenesis of Helicobacter pylori infection," (in eng), *Clin Microbiol Rev,* vol. 19, no. 3, pp. 449-90, Jul 2006, doi: 10.1128/cmr.00054-05.

[52] C. Burucoa and A. Axon, "Epidemiology of Helicobacter pylori infection," (in eng), *Helicobacter,* vol. 22 Suppl 1, Sep 2017, doi: 10.1111/hel.12403.

[53] B. Marshall, "Helicobacter pylori: 20 years on," (in eng), *Clin Med (Lond),* vol. 2, no. 2, pp. 147-52, Mar-Apr 2002, doi: 10.7861/clinmedicine.2-2-147.

[54] B. B. de Brito *et al.*, "Pathogenesis and clinical management of Helicobacter pylori gastric infection," (in eng), *World J Gastroenterol,* vol. 25, no. 37, pp. 5578-5589, Oct 7 2019, doi: 10.3748/wjg.v25.i37.5578.

[55] S. Suerbaum and P. Michetti, "Helicobacter pylori Infection," *The New England journal of medicine,* vol. 347, pp. 1175-86, 11/01 2002, doi: 10.1056/NEJMra020542.

[56] "World Gastroenterology Organisation Global Guideline: Helicobacter pylori in Developing Countries," *Journal of Clinical Gastroenterology,* vol. 45, no. 5, pp. 383-388, 2011, doi: 10.1097/MCG.0b013e31820fb8f6.
[57] A. K. Kamboj, T. G. Cotter, and A. S. Oxentenko, "Helicobacter pylori: The Past, Present, and Future in Management," (in eng), *Mayo Clin Proc,* vol. 92, no. 4, pp. 599-604, Apr 2017, doi: 10.1016/j.mayocp.2016.11.017.
[58] M. Zamani *et al.*, "Systematic review with meta-analysis: the worldwide prevalence of Helicobacter pylori infection," (in eng), *Aliment Pharmacol Ther,* vol. 47, no. 7, pp. 868-876, Apr 2018, doi: 10.1111/apt.14561.
[59] J. K. Y. Hooi *et al.*, "Global Prevalence of Helicobacter pylori Infection: Systematic Review and Meta-Analysis," *Gastroenterology,* vol. 153, no. 2, pp. 420-429, 2017/08/01/ 2017, doi: https://doi.org/10.1053/j.gastro.2017.04.022.
[60] M. Öztekin, B. Yılmaz, D. Ağagündüz, and R. Capasso, "Overview of Helicobacter pylori Infection: Clinical Features, Treatment, and Nutritional Aspects," (in eng), *Diseases,* vol. 9, no. 4, Sep 23 2021, doi: 10.3390/diseases9040066.
[61] J. Bastos *et al.*, "Sociodemographic determinants of prevalence and incidence of Helicobacter pylori infection in Portuguese adults," (in eng), *Helicobacter,* vol. 18, no. 6, pp. 413-22, Dec 2013, doi: 10.1111/hel.12061.
[62] C. Monteiro, A. R. Costa, and B. Peleteiro, "Sodium intake and Helicobacter pylori infection in the early stages of life," *Porto Biomedical Journal,* 10.1016/j.pbj.2016.05.001, doi: 10.1016/j.pbj.2016.05.001.
[63] I. A. Cardos *et al.*, "Evolution of Diagnostic Methods for Helicobacter pylori Infections: From Traditional Tests to High Technology, Advanced Sensitivity and Discrimination Tools," *Diagnostics,* vol. 12, p. 508, 02/16 2022, doi: 10.3390/diagnostics12020508.
[64] E. Tshibangu-Kabamba and Y. Yamaoka, "Helicobacter pylori infection and antibiotic resistance - from biology to clinical implications," (in eng), *Nat Rev Gastroenterol Hepatol,* vol. 18, no. 9, pp. 613-629, Sep 2021, doi: 10.1038/s41575-021-00449-x.
[65] W. K. Leung and D. Y. Graham, "Clarithromycin for Helicobacter pylori infection," (in eng), *Expert Opin Pharmacother,* vol. 1, no. 3, pp. 507-14, Mar 2000, doi: 10.1517/14656566.1.3.507.
[66] M. Sharaf *et al.*, "Co-delivery of hesperidin and clarithromycin in a nanostructured lipid carrier for the eradication of Helicobacter pylori in vitro," (in eng), *Bioorg Chem,* vol. 112, p. 104896, Jul 2021, doi: 10.1016/j.bioorg.2021.104896.
[67] L. Kuna, J. Jakab, R. Smolic, N. Raguz-Lucic, A. Vcev, and M. Smolic, "Peptic Ulcer Disease: A Brief Review of Conventional Therapy and Herbal Treatment Options," (in eng), *J Clin Med,* vol. 8, no. 2, Feb 3 2019, doi: 10.3390/jcm8020179.
[68] M. Keikha and M. Karbalaei, "Probiotics as the live microscopic fighters against Helicobacter pylori gastric infections," *BMC Gastroenterology,* vol. 21, no. 1, p. 388, 2021/10/20 2021, doi: 10.1186/s12876-021-01977-1.
[69] Z. Lv *et al.*, "Efficacy and safety of probiotics as adjuvant agents for Helicobacter pylori infection: A meta-analysis," *Exp Ther Med,* vol. 9, no. 3, pp. 707-716, 2015/03/01 2015, doi: 10.3892/etm.2015.2174.
[70] Y. Cong *et al.*, "Ureido-modified carboxymethyl chitosan-graft-stearic acid polymeric nano-micelles as a targeted delivering carrier of clarithromycin for

Helicobacter pylori: Preparation and in vitro evaluation," (in eng), *Int J Biol Macromol,* vol. 129, pp. 686-692, May 15 2019, doi: 10.1016/j.ijbiomac.2019.01.227.

[71] T. Safarov, B. Kiran, M. Bagirova, A. M. Allahverdiyev, and E. S. Abamor, "An overview of nanotechnology-based treatment approaches against Helicobacter Pylori," (in eng), *Expert Rev Anti Infect Ther,* vol. 17, no. 10, pp. 829-840, Oct 2019, doi: 10.1080/14787210.2019.1677464.

[72] A. Neshani, H. Zare, M. R. Akbari Eidgahi, A. Hooshyar Chichaklu, A. Movaqar, and K. Ghazvini, "Review of antimicrobial peptides with anti-Helicobacter pylori activity," *Helicobacter,* vol. 24, no. 1, p. e12555, 2019, doi: https://doi.org/10.1111/hel.12555.

[73] R. Spohn *et al.*, "Integrated evolutionary analysis reveals antimicrobial peptides with limited resistance," *Nature Communications,* vol. 10, no. 1, p. 4538, 2019/10/04 2019, doi: 10.1038/s41467-019-12364-6.

[74] K. Saravanakumar, R. Chelliah, D. MubarakAli, D. H. Oh, K. Kathiresan, and M. H. Wang, "Unveiling the potentials of biocompatible silver nanoparticles on human lung carcinoma A549 cells and Helicobacter pylori," (in eng), *Sci Rep,* vol. 9, no. 1, p. 5787, Apr 8 2019, doi: 10.1038/s41598-019-42112-1.

[75] V. Gopinath *et al.*, "Anti-Helicobacter pylori, cytotoxicity and catalytic activity of biosynthesized gold nanoparticles: Multifaceted application," *Arabian Journal of Chemistry,* vol. 12, no. 1, pp. 33-40, 2019/01/01/ 2019, doi: https://doi.org/10.1016/j.arabjc.2016.02.005.

[76] S. M. A. Sharaf, H. S. Abbas, and T. A. M. Ismaeil, "Characterization of spirugenic iron oxide nanoparticles and their antibacterial activity against multidrug-resistant Helicobacter pylori," *Egyptian Journal of Phycology,* vol. 20, no. 1, pp. 1-28, 2019, doi: 10.21608/egyjs.2019.116018.

[77] F. A. Khan, "Synthesis of Nanomaterials: Methods & Technology," in *Applications of Nanomaterials in Human Health*, F. A. Khan Ed. Singapore: Springer Singapore, 2020, pp. 15-21.

[78] Y. Liu *et al.*, "Formulation of Nanoparticles Using Mixing-Induced Nanoprecipitation for Drug Delivery," *Industrial & Engineering Chemistry Research,* vol. 59, no. 9, pp. 4134-4149, 2020/03/04 2020, doi: 10.1021/acs.iecr.9b04747.

[79] A. Zielińska *et al.*, "Polymeric Nanoparticles: Production, Characterization, Toxicology and Ecotoxicology," *Molecules,* vol. 25, p. 3731, 08/15 2020, doi: 10.3390/molecules25163731.

[80] Z. Tian, X. Ge, Y. Wang, and J. Xu, "Chapter 1 - Nanoparticles and Nanocomposites With Microfluidic Technology," in *Polymer-Based Multifunctional Nanocomposites and Their Applications*, K. Song, C. Liu, and J. Z. Guo Eds.: Elsevier, 2019, pp. 1-33.

[81] D. M. K.M, B. Shivakumar, and P. Kumar, "Microencapsulation: An Acclaimed Novel Drug-Delivery System for NSAIDs in Arthritis," *Critical reviews in therapeutic drug carrier systems,* vol. 27, pp. 509-45, 01/01 2010, doi: 10.1615/CritRevTherDrugCarrierSyst.v27.i6.20.

[82] S. Pedroso-Santana and N. Fleitas-Salazar, "Ionotropic gelation method in the synthesis of nanoparticles/microparticles for biomedical purposes," *Polymer International,* vol. 69, no. 5, pp. 443-447, 2020, doi: https://doi.org/10.1002/pi.5970.

[83] S. Exarhopoulos, A. Goulas, and G. Dimitreli, "Biodegradable Films from Kefiran-Based Cryogel Systems," *Macromol,* vol. 2, no. 3, pp. 324-345, 2022. [Online]. Available: https://www.mdpi.com/2673-6209/2/3/21.

[84] D. R. Fonseca *et al.*, "Grafting MSI-78A onto chitosan microspheres enhances its antimicrobial activity," (in eng), *Acta Biomater,* vol. 137, pp. 186-198, Jan 1 2022, doi: 10.1016/j.actbio.2021.09.063.

[85] C. Patino, "Alginate Hydrogel as a Three-dimensional Extracellular Matrix for In Vitro Models of Development," 11/01 2013.

[86] P. Parreira *et al.*, "Surface Grafted MSI-78A Antimicrobial Peptide has High Potential for Gastric Infection Management," *Scientific Reports,* vol. 9, 12/03 2019, doi: 10.1038/s41598-019-53918-4.

[87] I. C. Gonçalves, A. Magalhães, M. Fernandes, I. V. Rodrigues, C. A. Reis, and M. C. Martins, "Bacterial-binding chitosan microspheres for gastric infection treatment and prevention," (in eng), *Acta Biomater,* vol. 9, no. 12, pp. 9370-8, Dec 2013, doi: 10.1016/j.actbio.2013.07.034.

[88] C. L. Seabra *et al.*, "Lipid nanoparticles to counteract gastric infection without affecting gut microbiota," *European Journal of Pharmaceutics and Biopharmaceutics,* vol. 127, pp. 378-386, 2018/06/01/ 2018, doi: https://doi.org/10.1016/j.ejpb.2018.02.030.

[89] C. L. Seabra *et al.*, "Lipid nanoparticles to counteract gastric infection without affecting gut microbiota," (in eng), *Eur J Pharm Biopharm,* vol. 127, pp. 378-386, Jun 2018, doi: 10.1016/j.ejpb.2018.02.030.

[90] P. C. Henriques *et al.*, "Orally administrated chitosan microspheres bind Helicobacter pylori and decrease gastric infection in mice," (in eng), *Acta Biomater,* vol. 114, pp. 206-220, Sep 15 2020, doi: 10.1016/j.actbio.2020.06.035.

[91] Z. Chen, J. Shi, X. Yang, Y. Liu, B. Nan, and Z. Wang, "Isolation of exopolysaccharide-producing bacteria and yeasts from Tibetan kefir and characterisation of the exopolysaccharides," *International Journal of Dairy Technology,* vol. 69, pp. n/a-n/a, 08/01 2016, doi: 10.1111/1471-0307.12276.

[92] O. McAuliffe, R. P. Ross, and C. Hill, "Lantibiotics: structure, biosynthesis and mode of action," (in eng), *FEMS Microbiol Rev,* vol. 25, no. 3, pp. 285-308, May 2001, doi: 10.1111/j.1574-6976.2001.tb00579.x.

[93] M. Bernela, P. Kaur, M. Chopra, and R. Thakur, "Synthesis, characterization of nisin loaded alginate–chitosan–pluronic composite nanoparticles and evaluation against microbes," *LWT - Food Science and Technology,* vol. 59, pp. 1093-1099, 12/01 2014, doi: 10.1016/j.lwt.2014.05.061.

[94] J. Kong and S. Yu, "Fourier transform infrared spectroscopic analysis of protein secondary structures," (in eng), *Acta Biochim Biophys Sin (Shanghai),* vol. 39, no. 8, pp. 549-59, Aug 2007, doi: 10.1111/j.1745-7270.2007.00320.x.

[95] J. Pierna, O. Abbas, P. Dardenne, and V. Baeten, "Discrimination of Corsican honey by FT-Raman spectroscopy and chemometrics," *Biotechnologie, Agronomie, Société et Environnement,* vol. 15, pp. 75-84, 2011.

[96] L. F. C. de Oliveira, R. Colombara, and H. G. M. Edwards, "Fourier Transform Raman Spectroscopy of Honey," *Appl. Spectrosc.,* vol. 56, no. 3, pp. 306-311, 2002/03/01 2002. [Online]. Available: https://opg.optica.org/as/abstract.cfm?URI=as-56-3-306.

[97] S. Schlücker, "Confocal Raman Microscopy. Thomas Dieing, Olaf Hollricher, and Jan Toporski (Eds.)," *Microscopy and Microanalysis,* vol. 18, no. 6, pp. 1494-1494, 2012, doi: 10.1017/S1431927612011853.

[98] B. L. Hsu, Y. M. Weng, Y. H. Liao, and W. Chen, "Structural investigation of edible zein films/coatings and directly determining their thickness by FT-Raman spectroscopy," (in eng), *J Agric Food Chem,* vol. 53, no. 13, pp. 5089-95, Jun 29 2005, doi: 10.1021/jf0501490.

[99] P. Zimet *et al.*, "Optimization and characterization of nisin-loaded alginate-chitosan nanoparticles with antimicrobial activity in lean beef," *Lwt - Food Science and Technology,* vol. 91, pp. 107-116, 2018.

[100] Y. Wang, C. Li, P. Liu, Z. Ahmed, P. Xiao, and X. Bai, "Physical characterization of exopolysaccharide produced by Lactobacillus plantarum KF5 isolated from Tibet Kefir," *Carbohydrate Polymers,* vol. 82, no. 3, pp. 895-903, 2010/10/15/ 2010, doi: https://doi.org/10.1016/j.carbpol.2010.06.013.

[101] J. D. Clogston and A. K. Patri, "Zeta potential measurement," (in eng), *Methods Mol Biol,* vol. 697, pp. 63-70, 2011, doi: 10.1007/978-1-60327-198-1_6.

[102] I. Braccini and S. Pérez, "Molecular basis of C(2+)-induced gelation in alginates and pectins: the egg-box model revisited," (in eng), *Biomacromolecules,* vol. 2, no. 4, pp. 1089-96, Winter 2001, doi: 10.1021/bm010008g.

[103] A. L. P. Cartaxo, "Nanoparticles types and properties – understanding these promising devices in the biomedical area," 2015.

[104] N. P. Santisteban, M. R. Morrow, and V. Booth, "Effect of AMPs MSI-78 and BP100 on the lipid acyl chains of 2H-labeled intact Gram positive bacteria," *Biochimica et Biophysica Acta (BBA) - Biomembranes,* vol. 1862, no. 5, p. 183199, 2020/05/01/ 2020, doi: https://doi.org/10.1016/j.bbamem.2020.183199.

[105] G. A. Pankey and L. D. Sabath, "Clinical Relevance of Bacteriostatic versus Bactericidal Mechanisms of Action in the Treatment of Gram-Positive Bacterial Infections," *Clinical Infectious Diseases,* vol. 38, no. 6, pp. 864-870, 2004, doi: 10.1086/381972.

[106] J. Tomas *et al.*, "Early colonizing Esche richia coli elicits remodeling of rat colonic epithelium shifting toward a new homeostatic state," *The ISME Journal,* vol. 9, no. 1, pp. 46-58, 2015/01/01 2015, doi: 10.1038/ismej.2014.111.

[107] C. Anutrakunchai, J. G. M. Bolscher, B. P. Krom, S. Kanthawong, S. Chareonsudjai, and S. Taweechaisupapong, "Impact of nutritional stress on drug susceptibility and biofilm structures of Burkholderia pseudomallei and Burkholderia thailandensis grown in static and microfluidic systems," (in eng), *PLoS One,* vol. 13, no. 3, p. e0194946, 2018, doi: 10.1371/journal.pone.0194946.

[108] S. Nam, R. Stowers, J. Lou, Y. Xia, and O. Chaudhuri, "Varying PEG density to control stress relaxation in alginate-PEG hydrogels for 3D cell culture studies," (in eng), *Biomaterials,* vol. 200, pp. 15-24, 2019/04// 2019, doi: 10.1016/j.biomaterials.2019.02.004.

[109] B. Kowalska-Krochmal and R. Dudek-Wicher, "The Minimum Inhibitory Concentration of Antibiotics: Methods, Interpretation, Clinical Relevance," (in eng), *Pathogens,* vol. 10, no. 2, Feb 4 2021, doi: 10.3390/pathogens10020165.

[110] N. V. Ballal, M. Kundabala, S. Bhat, N. Rao, and B. S. S. Rao, "A comparative in vitro evaluation of cytotoxic effects of EDTA and maleic acid: Root canal irrigants," *Oral Surgery, Oral Medicine, Oral Pathology, Oral Radiology, and Endodontology,* vol. 108, no. 4, pp. 633-638, 2009/10/01/ 2009, doi: https://doi.org/10.1016/j.tripleo.2009.05.039.

[111] V. Kuete, O. Karaosmanoğlu, and H. Sivas, "Chapter 10 - Anticancer Activities of African Medicinal Spices and Vegetables," in *Medicinal Spices and Vegetables from Africa*, V. Kuete Ed.: Academic Press, 2017, pp. 271-297.

[112] J. S. H. Seah, S. Singh, L. P. Tan, and D. Choudhury, "Scaffolds for the manufacture of cultured meat," (in eng), *Crit Rev Biotechnol,* vol. 42, no. 2, pp. 311-323, Mar 2022, doi: 10.1080/07388551.2021.1931803.
[113] T. G. Mezger, "The Rheology Handbook: For users of rotational and oscillatory rheometers," 2020.
[114] C. Yan and D. J. Pochan, "Rheological properties of peptide-based hydrogels for biomedical and other applications," (in eng), *Chem Soc Rev,* vol. 39, no. 9, pp. 3528-40, Sep 2010, doi: 10.1039/b919449p.